# CHAPTER II
# LITERATURE REVIEW

## 2.1 Drilling

### 2.1.1 The Fundamental Drilling Concept

The basic drilling process is simple. A bit rotates at the bottom of a string of pipe, called the drillstring, to grind a hole through the rock layers (Figure 2.1). A fluid called drilling mud which is a suspension of chemicals and minerals in water or oil circulates through the drill bit. The mud is used to lubricate and cool the bit, remove rock cuttings, and prevent collapse of the well bore (Bott and Carson, 2007). As the bit penetrates deeper, the crew threads additional pipe, called a casing, onto the top of the string. There are basically six types of casing strings: conductor casing, surface casing, intermediate casing, production casing, liners and tieback strings (Mitchell *et al.*, 1988). The casing's diameter and wall thickness are various depending on well depth and type as shown in Figure 2.2.

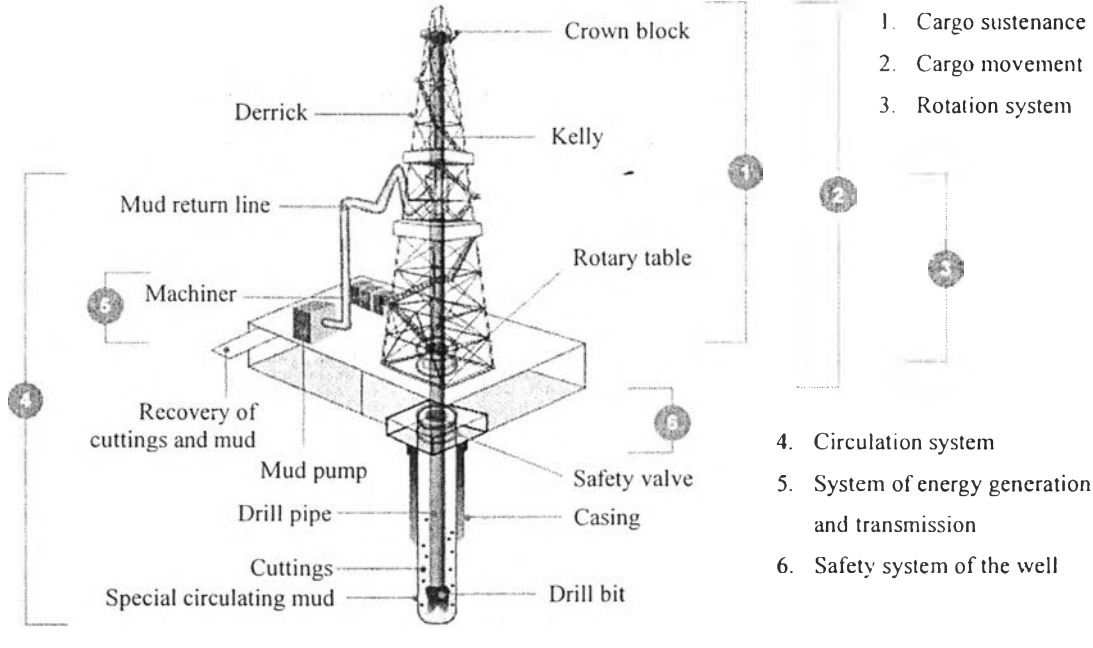


**Figure 2.1** Rotary drilling rig component (http://www.galpenergia.com/EN/Investidor/ConhecerGalpEnergia/Os-nossos-negocios/ExploracaoProducao/fundamentos-engenharia-petroleo/Paginas/Perfuracao.aspx).

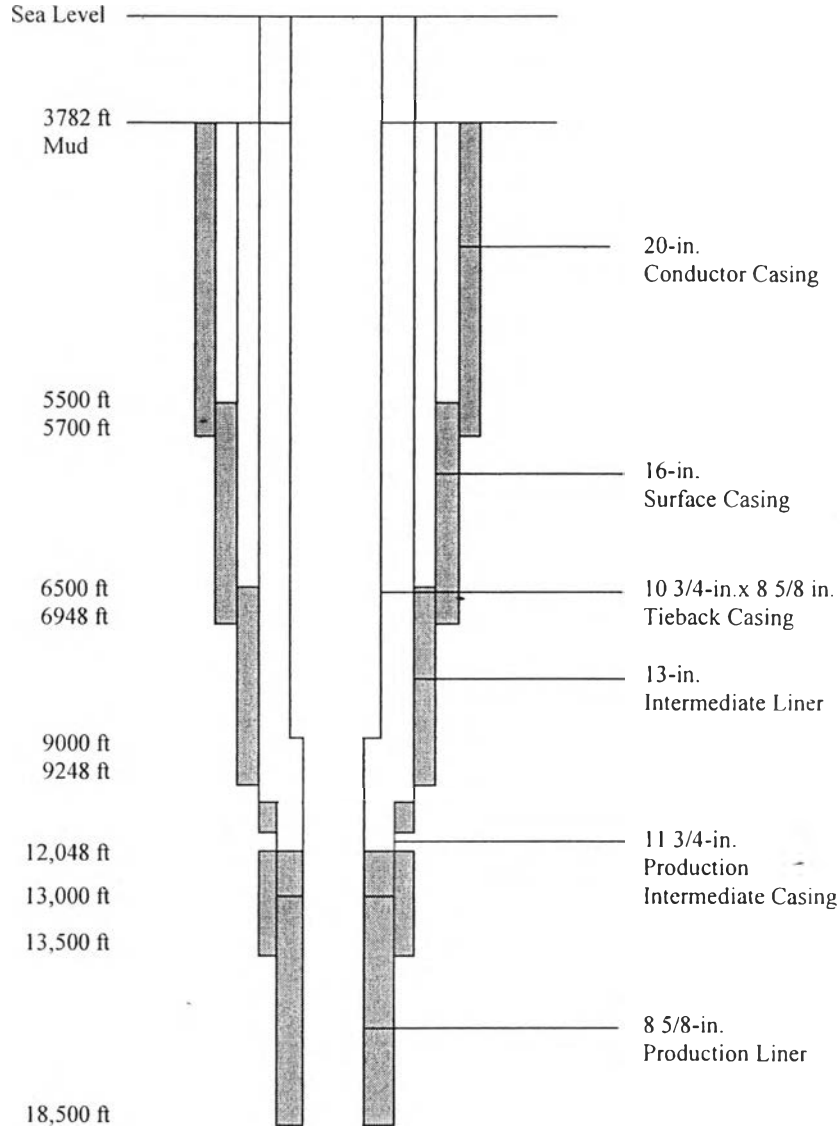


**Figure 2.2** Offshore casing design (Mitchell *et al.*, 1988).

2.1.2 Drilling Activities

Normally, drilling activities can be occurred by many purposes going to successful well such as drilling with no, or neglected, movements in axial direction referred as rotating-off bottom (RoffB), drilling with engagement of a bit and formation referred as rotating-on bottom (RonB), tripping out without rotation referred as pulling out of the hole (POOH), and tripping in without rotation referred as running into the hole (RIH).

*2.1.2.1 Rotating Operation*

Rotating off-bottom operates by rotating the drillstring without any axial movement. There is no weight on bit (WOB) or torque on bit (TOB) because the bit is not engaged with formation. Drilling is in this context to enlarge the wellbore by rotating the drillstring and bit on bottom of the wellbore as rotating on-bottom. The velocity in axial direction (rate of penetration, ROP) is much smaller than the rotational speed (round per minute, RPM) and the situation can be seen as a case with drillstring rotation without axial movement.

*2.1.2.2 Tripping Operation*

Tripping is moving the drillpipe without rotation and circulation, and is often measured while the drillpipe is pulled out of hole and before making a connection. Measurements from operation without rotation are helpful to apply to analyze the downhole situation due to the full friction, which is acting in the axial movement and affecting the hookload whether it is maximum (Kucs et al. 2008). Measured hookload at the surface can indicate the friction, which is force needed to move the drillpipe up or down, by studying the deviation in tension when going in and out with the drillstring.

*2.1.2.3 Sliding Operation*

Sliding operation is referred to drilling with a mud motor rotating the bit downhole without rotating the drillstring from the surface. The bottomhole assembly (BHA) is fitted with a bent sub or a bent housing mud motor, or both, for directional drilling.

2.1.3 Directional Drilling

Directional drilling is an inclined drilling to the pay zone (Figure 2.3) allowing a number of wells to be drilled from one location on the surface. Horizontal wells can penetrate a long section of the rock formation, revealing more of the reservoir to the wellbore. This reduces the time it takes to extract crude oil or natural gas from the reservoir and in some cases increases the total amount of product that can be recovered. As drilling technologies and methods continue to improve, the reach of wells into producing formations continues to increase.

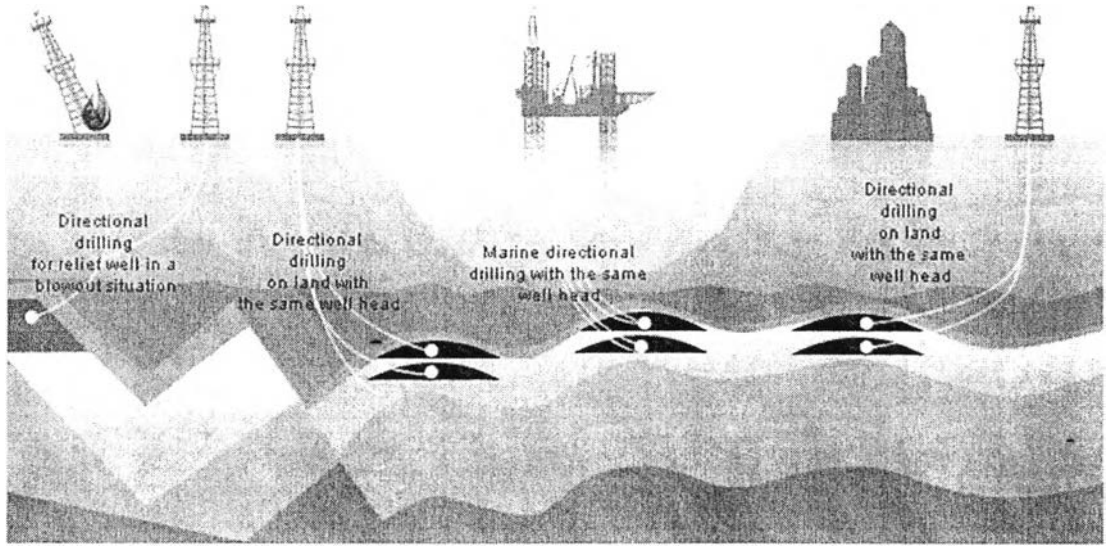


**Figure 2.3** The trajectory of the directional well (http://www.galpenergia.com).

The directional wellbore trajectory described as follow:

- Measured depth (MD) is the distance measured along the well path from one reference point to the survey point (Figure 2.4).
- The true vertical depth (TVD) is distance from a point in the well (usually the current or final depth) to a point at the surface (Figure 2.4), usually the elevation of the rotary kelly bushing (RKB).
- Inclination ($\theta$) is the angle between vertical and the tangent to the wellbore. A vertical well would be zero degree; a horizontal well would be 90 degrees.
- Azimuth ($\phi$) is the angle between true north and a tangent to the wellbore projected to a horizontal plane (Figure 2.4). It starts from zero which is north and moves clockwise. West is then 270 degrees.
- Dogleg severity (DLS) is a measure of the amount of change in the inclination, and/or azimuth of a borehole, usually expressed in degrees per 30 feet.
- Kick off point (KOP) is defined as the point below the surface location from where the well is deflected from the vertical as well as the beginning of build section (Figure 2.5).

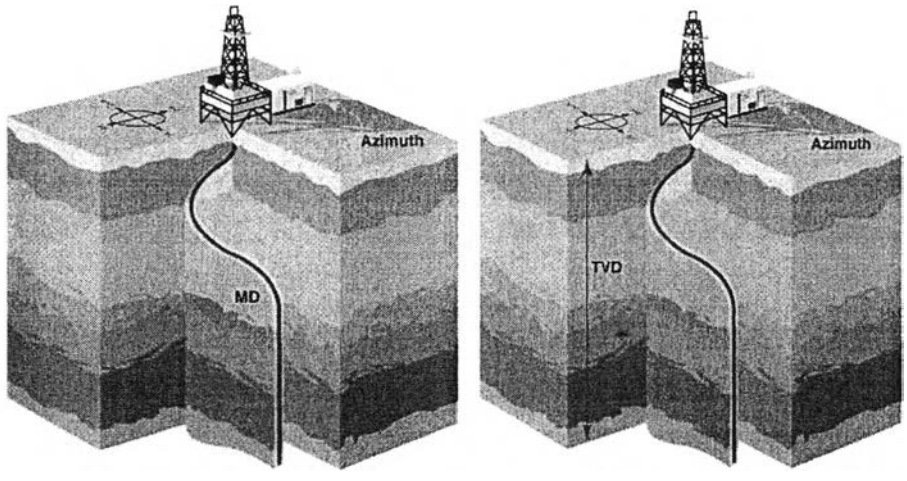


**Figure 2.4** The real well trajectory (http://directionaldrilling.blogspot.com).

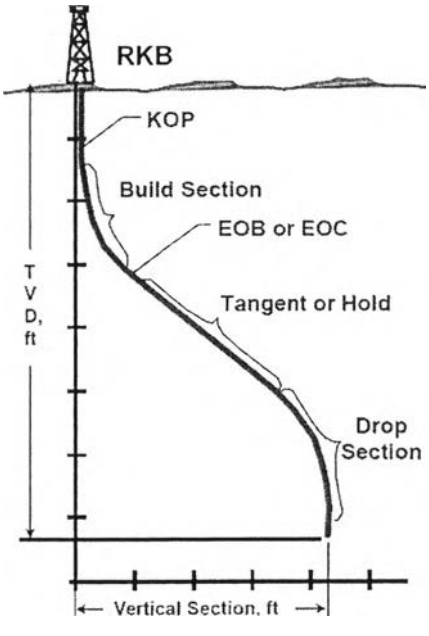


**Figure 2.5** A simple build/hold/drop well terminology.
(http://directionaldrilling.blogspot.com)

- Build section is a portion of the hole in which the inclination angle is increased.
- Build up rate (BUR) is simply the measured change in angle divided by the measured depth (MD) drilled and normally expressed in terms of degrees per hundred feet (deg/100 ft).

- End of build (EOB) is the desired hole angle is achieved (Figure 2.5).
- Drop off is the act of reducing the inclination of the drilled hole to vertical.
- Drop section is portion of the hole in which the inclination angle is decreased (Figure 2.5).
- Drop off rate is the rate of change of the inclination in the part of the wellbore where the inclination angle is purposely returned toward vertical, usually expressed in degrees per feet.
- Hold is act of maintaining the inclination and azimuth of the wellbore to remain constant.
- Tangent or hold section is the portion of hole in which the inclination and azimuth is maintained the same.

The development of longer reach wells, especially extended reach drillings (ERD) is the ratio of the measured depth (MD) of the well divided by the true vertical depth (TVD) greater than 2 (Agbaji, 2011). It becomes very important not only to drain older fields more efficiently but also to reduce the number of vertical wells and economic point of view (Aadnoy and Andersen, 1998).

Excessive torque and drag can be vital issues in directional drilling, including tight-hole conditions, sloughing shale, key seats, differential sticking, cuttings build-up. These caused by poor hole cleaning and sliding wellbore friction. On the other hand, in wells with good hole conditions, the primary source of torque and drag is sliding friction (Johancsik *et al.*, 1984).

## 2.2 Drilling Processes

A challenging well can cost about US$30 million (Sui *et al.*, 2012), not including the costs associated with the risk of drilling hazards. The other important consideration in the drilling industry is the reduction of potential of drilling hazards and drilling operation costs by decrease in NPT and lower risk of damaged drilling equipment. Drilling companies and operators apply several pre-drill planning

processes and methods to diminish those risks. In planned drilling processes, there are a series of steps and operations that go into completing a successful well.

The well planning process is aim to review offset well data for details of events that are relevant to the drilling of the new well. This can be a very time-consuming task, particularly if there are a number of wells available locally (Deeks *et al.*, 2012). Also, it is often unclear whether events recorded in one well are of direct relevance to the current well. Although the drilling service companies use the latest technology and equipment, it is evident that the involvement of planning process leads to a better and dependable technique resulting in identifying the risk hazards and in developing an optimum strategy.

Aldawood *et al.* (2011) introduced a workflow, integrated pre-well planning (IPWP), which has been designed and tested in service company incorporation in order to enhance the drilling operation efficiently. The most important role within this process is the involvement and cooperation amongst various application teams with individual expertise. This process is widely divided into three main phases: planning, operational analysis, and post well analysis (Figure 2.6).

This research focuses on planning phase (Figure 2.7). At the beginning, objectives are set by both the customer and the service company. Generally, the customer defines the overall objectives and work scope, and the service companies choose their working strategy to set their targets accordingly.

Gathering data are based on the objectives of the project, such as project, location, formation lithology, and well profile etc.

Identification of offset wells is started by looking for wells in the same field, or in a close geographical proximity. As a normal practice, three or four wells drilled recently in the same structure and use of the latest drilling technology, are taken into consideration for thorough study.

For conducting task meeting to establish responsibility, once the offset wells have been identified and studied thoroughly, a task meeting is arranged where personnel from various departments give their input in the front of suggestions, recommendations and requests.

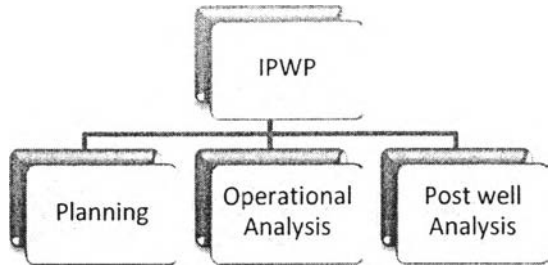


**Figure 2.6** Integrated pre well planning (IPWP) main phase's process (Aldawood *et al.*, 2011).

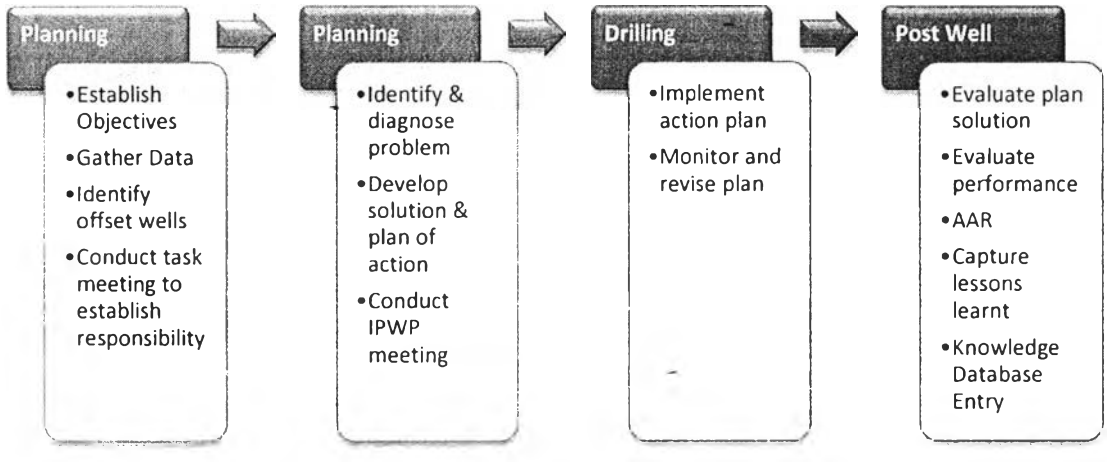


**Figure 2.7** Integrated pre well planning (IPWP) work flow (Aldawood *et al.*, 2011).

Identification and diagnosis of problem for past case is a critical aspect in being able to identify risks and challenges. Major risks involved are stuck pipe, lost circulation, hole conditions (torque and drag), equivalent circulating density (ECD) monitoring, $H_2S$, formation pressure, and bottom hole assembly (BHA) selection.

For a developing solution and plan of action, at this point, it is vital to develop a solution and plan of action by understanding sources of risks and challenges involved, and the methods to overcome them.

For conducting IPWP meeting, this process is of the almost importance where all personnel gather to discuss the outputs after having followed all above steps, and create a threshold of drilling practices and daily operational procedures to

be carried out by personnel of all departments. The company man is also briefed about the procedure, as he will be involved with the operations directly.

## 2.3 Fundamental Concept of Torque and Drag

The torque and drag (T&D) modeling is a fundamental analysis tool in well planning because it helps to predict and prevent drilling problems that might occur during the drilling process and also well completion. Although T&D software has existed since the 1990s, some confusion still exists over the validity of the models that are used to characterize drilling operations, especially when the length of modern horizontal wells is extended (Mason and Chen, 2007).

### 2.3.1 Torque

When referred to torque and drilling, the torque is a moment required to rotate the drillstring to overcome the rotational friction between the drillstring and casing/open hole in the well known as frictional torques (Figure 2.8). The surface torque comprises of frictional torques, dynamic torques, mechanical torques and bit torque. The viscous force between drillstring and drilling fluid is called dynamic torque. The mechanical torque is owing to cutting beds, borehole ledges and stabilizer effects, and the bit torque is generated by the impact on the formation (Payne and Abbassian, 1997). Following aspects are often deciding the magnitude of the torque (Bennetzen *et al.*, 2010): tension or compression in the drillstring, dogleg severity (DLS), sizes of the drillstring and wellbore, weight of the string, directional changes of the wellbore (inclination and azimuth), and lubricity or friction factor.

High torque and high drag forces normally occurs together (Tveitdal, 2011). In a directional well or extended reach well, torque is a major limiting factor to how long it can be drilled, as it eventually will defeat the hoisting equipment or drillstrings limitation (Stuart *et al.*, 2003). Torque is directly proportional to the radius of which rotation occurs and the coefficient of friction and the normal force of which the pipe has against the wellbore.

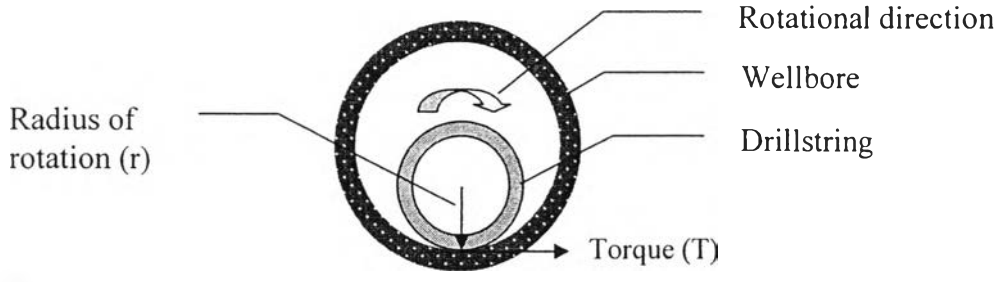


**Figure 2.8** Torque (T) to rotate the drillstring in the wellbore (Tveitdal, 2011).

2.3.2 Drag

The drag is the force required to move the drillstring up or down axially in the hole and also used to overcome the axial friction in the well. This is a phenomenon associated with deviated wells. Compared to vertical wells, horizontal and extended reach wells present a series of additional and increased challenges related to getting the drillstring to bottom. The most fundamental difference is the fact that the portion of the drillstring in high angle and lateral sections will no longer slide down with gravity but have to be pushed by the casing above it. The forces act on the drillstring as illustrated in Figure 2.9 (Sanchez and Adams, 2012).

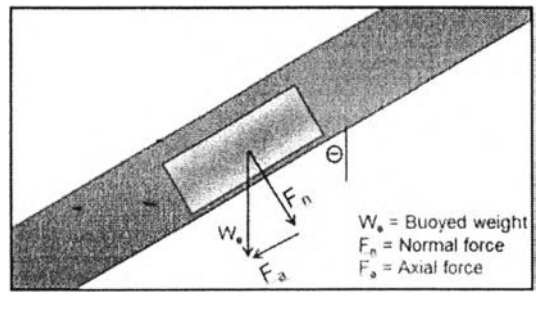


**Figure 2.9** Normal ($F_n$) and axial ($F_a$) forces (Sanchez and Adams, 2012).

The normal contact ($F_n$) and axial forces ($F_a$) can be calculated as:

$$F_n = W_e sin(\theta) \tag{2.1}$$

$$F_a = W_e cos(\theta) \tag{2.2}$$

Where $W_e$ is a unit buoyed weight of the drillstring in drilling fluid and $\theta$ is an angle of inclination. The buoyed weight is the unit weight of the drillstring in air multiplied with the buoyancy factor.

The buoyancy factor ($\beta$) is defined by equation (2.3) which is a different fluid inside and outside of the drillpipe (Aadnoy and Kaarstad, 2006). Otherwise, there is equal fluid density inside and outside of the drillpipe, it is reduced to equation (2.4).

$$\beta = 1 - \frac{\rho_0 A_0 - \rho_i A_i}{\rho_{pipe}(A_0 - A_i)} \tag{2.3}$$

$$\beta = 1 - \frac{\rho_0}{\rho_{pipe}} \tag{2.4}$$

Where $\rho_0$ is a density of fluid outside and $\rho_i$ is a density of fluid inside of the drillpipe. $A_0$ is a annulus cross sectional area of outside and $A_i$ is a cross sectional area of inside of the drillpipe. $\rho_{pipe}$ is a density of the drillpipe material.

For the drillstring to slide down, the axial force, $F_a$, must be larger than the drag force, $F_d$. The drag force would be theoretically calculated as:

$$F_d = \mu F_n \tag{2.5}$$

Where $\mu$ is a friction factor. This value is between 0.20 and 0.60 (Sanchez and Adams, 2012). Drag is directly proportional to the normal force, friction factor and drillstring movement by equation (2.6) (McCormick *et al.*, 2012). Torque is also directly proportional to the normal force, friction factor, radius about which torque is generated and drillstring movement by equation (2.7).

$$F_d = F_n \times \mu \times \left(\frac{V_t}{V}\right) \tag{2.6}$$

$$T = F_n \times r_t \times \mu \times \left(\frac{V_r}{V}\right) \tag{2.7}$$

Where:

| | | |
|---|---|---|
| $F_d$ | = | drag force, lbf |
| $F_n$ | = | normal force, lbf |
| T | = | torque, ft-lbf |
| μ | = | coefficient of friction |
| $\tau$ | = | trip speed, ft/min |
| $V$ | = | resultant speed $\sqrt{V_t{}^2 + V_r{}^2}$, ft/min |
| $V_r$ | = | angular speed = diameter × π × RPM/60, ft/min |
| $r_t$ | = | radius about which rotation occurs, ft |

2.3.3 Normal force

The torque and drag equations both consist of the normal force. The normal force is an opposing force to the side load against the borehole in the perpendicular direction as shown in Figure 2.10. Theoretically, the normal force in an entirely vertical section of the borehole is zero, though some sections of the drillstring will touch the borehole. Therefore, the normal force in the vertical section can be small, but never be zero (McCormick *et al.*, 2012).

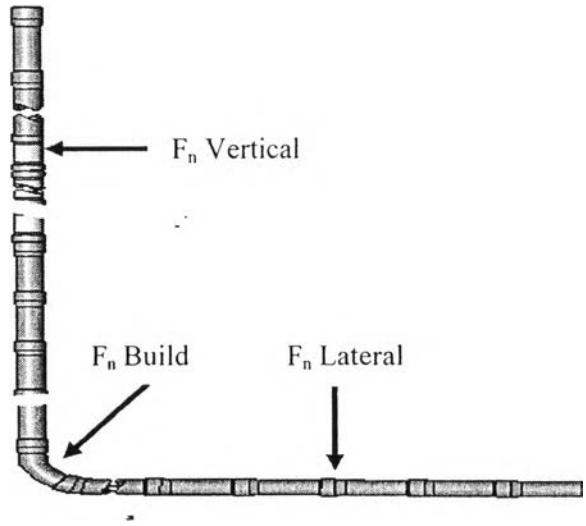


**Figure 2.10** Drillstring with the normal contact force (McCormick *et al.*, 2011).

2.3.4 Friction factor

Generally, the fiction factor or the coefficient of friction is expressed, the definition in equation (2.8) as a scalar dimensionless number between zero and one. The friction force will also increase friction as the coefficient is increased.

$$\mu = \frac{F_d}{F_n} \tag{2.8}$$

It is common to refer to two different friction factors; static friction and dynamic friction, or kinetic friction, as illustrated in Figure 2.11. As a force is applied to an object, the region for static friction last until the force is great enough to overcome the initial resistance to move the object. Kinetic friction is on the other hand valid for objects in movement, and is the one used in torque & drag models. The static friction on the other hand can be associated with differential sticking environment, which is a situation where the string is sucked into the borehole wall because of higher pressure in the wellbore than the pressure in the formation (Mason and Chen, 2007). The static friction is in general larger than the dynamic, however in many wells static and dynamic friction can be difficult to distinguish.

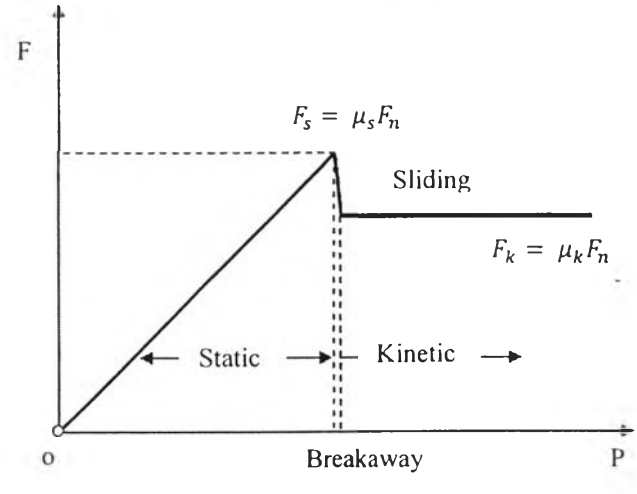


**Figure 2.11** Region of static friction and dynamic friction as a function of pulling force (Samuel, 2010).

The coefficient of friction is involved with torque and drag analysis. Friction factors that are generated by matching actual hookload and surface torque values are extremely useful for predicting loads further down the hole. Any predicted values will be inaccurate because of the complexity and multitude of variables that affect the friction factor (Long *et al.*, 2009). The actual coefficient of friction used in a T&D model takes into account many environmental factors, such as micro-tortuosity, drilling fluid type and composition, and formation type in the open hole section and casing condition in the cased hole section (Gynor *et al.*, 2002). For this reason, when the coefficient of friction is used in a model, it is often referred to as a friction factor as shown in Table 2.1.

Often T&D modelings have specific friction factors that are commonly used as assumptions which will assist of well and operation planning. One example is a default value of 0.22 for the casing hole friction factor (CHFF) and 0.30 for the open hole friction factor (OHFF) (McCormick *et al.*, 2012).

**Table 2.1** Range of friction factors (Samuel, 2010)

| Fluid Type | Friction Factor | |
|---|---|---|
| | Cased hole | Open hole |
| Oil-based | 0.16-0.20 | 0.17-0.25 |
| Water-based | 0.25-0.35 | 0.25-0.40 |
| Brine | 0.30-0.4 | 0.3-0.4 |
| Polymer-based | 0.15-0.22 | 0.2-0.3 |
| Synthetic-based | 0.12-0.18 | 0.15-0.25 |
| Foam | 0.30-0.4 | 0.35-0.55 |
| Air | 0.35-0.55 | 0.40-0.60 |

2.3.5 Measurement of Torque and Drag

The true field measured values of torque and drag always have some influence from other contributions. Some parameters can be modeled, while other effects are lumped together into the fudge factor which called a friction factor, which is not the same as the friction coefficient as in pure kinetic sliding friction. The combined effect of all parameters gives the total torque and drag forces (Johancsik *et al.*, 1984).

The drag is found by use of a weight indicator of the hookload on the rig, while measures the weight on bit (WOB), the drag and over-pull forces. This is usually an accurate and repeatable method. Measurements of the hookload are read from the tension in the deadline. The deadline is attached to the deadline anchor as seen in Figure 2.12. The hook load is not directly read from the deadline, but is a function of the deadline tension and number of lines, n, between the sheaves (Luke and Juvkam-Wold, 1992). Moreover, this simple relationship does not account for friction effects or movement direction. The accurate hookload should account for sheave efficiency.

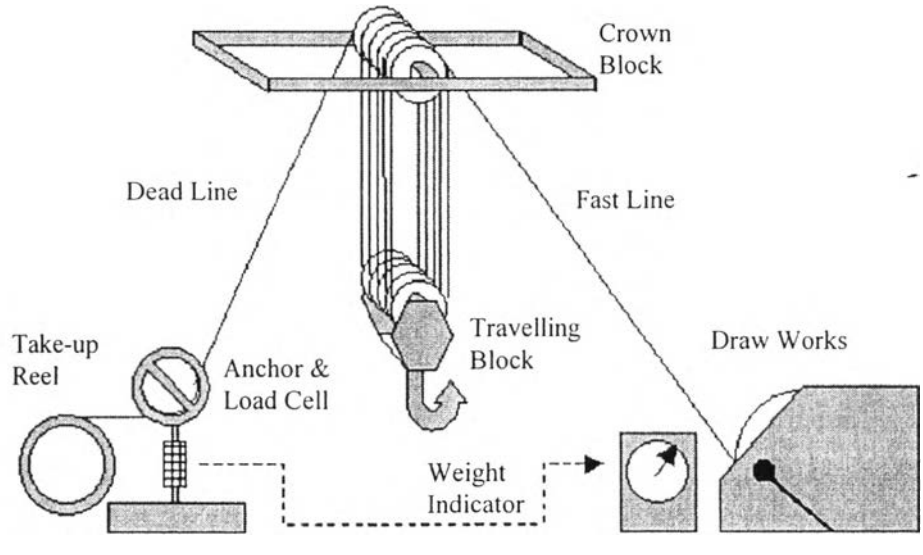


**Figure 2.12** An overview of the hoisting system (Luke and Juvkam-Wold, 1992).

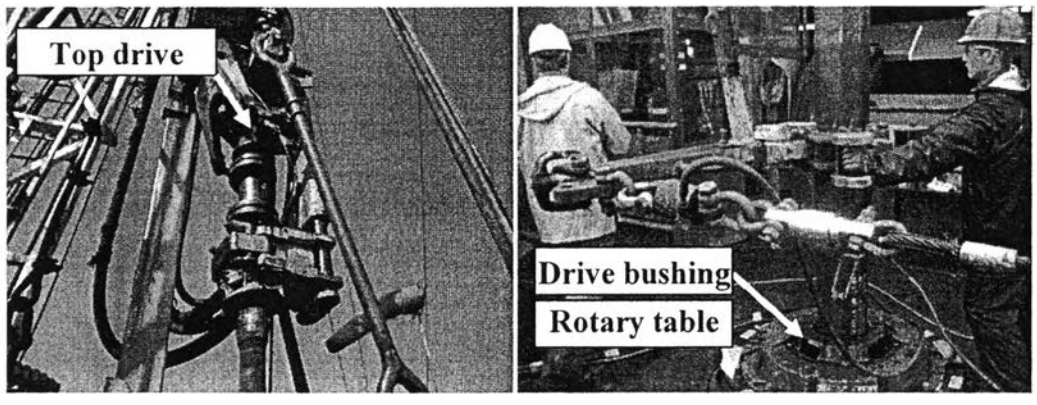


**Figure 2.13** Top drive and rotary table of a rig providing a torque to the drillstring.

The torque is, on the other hand, much more difficult to get reliable reading on, where a portable torque meter is placed between the rotary table and the drive bushing, but the development of sensors of torque can be measured at the top drive accurately (Figure 2.13). The apparatus provides oscillating values where an average value must be used.

## 2.4 Torque and Drag Model

### 2.4.1 Soft String Model

In 1980s, Johancsik *et al.* developed the first T&D software programs known as the soft string model. A soft string model assumes that the entire drillstring lies against the wellbore, and the stiffness of the drillstring is not accounted for. The drillstring is modeled as a weighted cable (Mason and Chen, 2007) that is divided into short elements (Figure 2.14) that its shape conforms to the shape of the wellbore. The forces acting on the elements consist of tension, compression, and torsion that cumulatively build from the bottom of the string to the surface. In other words, torque and drag are calculated by summing the segments of the torque and drag generated from bottom of the string to the surface. Due to the disregard of the bending stiffness and radial clearance of the drill string, there are some arguments of the accuracy of the soft string model. However, depending on the well situation, the soft string model may be closer to field data than stiff string model or vice versa (McCormick *et al.*, 2011).

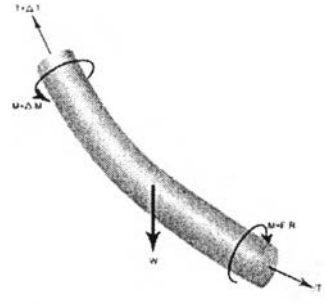

**Figure 2.14** Short elements in a drillstring (McCormick *et al.*, 2011).

Johancsik *et al.* (1984) determined the torque radius for the moment arm to be two-thirds of the distance between pipe body radius and tool joint radius. It was a reasonable assumption that two-thirds of the side load is carried by tool joints and one-third is carried by the pipe body. Others have used the tool joint radius as the torque radius, based on the assumption that the entire side load, or contact force, is carried by tool joints, which effectively means the pipe body is not in contact at all with the wellbore (Tikhonov *et al.*, 2013).

### 2.4.2 Stiff String Model

In addition to soft string modeling, stiff string T&D models have also been developed to overcome the soft string models. One major difference between the soft string model and the stiff string model is that it accounts for the bending stiffness of the string including radial clearance in the wellbore as well. The stiff string models are most beneficial when wells have high tortuous trajectories, high dogleg severity, or stiff tubular (McCormick *et al.*, 2011).

The stiff string model is more complex than the soft string model because of the additional inputs and calculations needed to account for various bending forces. A greater variety of numerical methods including finite difference, finite element and semi analytical techniques, are employed in the stiff string modeling programs (Mason and Chen, 2007). It attempts to give a more realistic torque and drag analysis on more difficult well. Nevertheless, it is hard to accurately account for tubular bending forces and radial clearance.

Although the stiff string models incorporate more variables, it is not necessarily more accurate than the soft string model. The soft string model is used because of the simplicity of its algorithm, rapid calculation time on even the most basic laptop computer, and the sufficiently accurate results obtained for many common drilling situations (Tikhonov *et al.*, 2013). Proponents of soft string models argue the difference between the soft and the stiff string models that the former uses one large guess, the friction factor while the latter uses many small guesses (McCormick *et al.*, 2011).

### 2.3.3 Tortuosity Effect

Tortuosity occurs when the actual well bore deviates from the planned trajectory, in a horizontal direction. Extended reach wells tend to have more tortuous wellbores. The effects include high torque and drag, poor hole cleaning, and drillstring buckling (Gaynor *et al.*, 2001).

Gaynor *et al.* (2001) explained the difference between tortuosity and micro-tortuosity that there are three tortuosities: planned tortuosity ($T_p$), large scale tortuosity ($T_l$) and micro-tortuosity ($T_m$). Firstly, the planned tortuosity is the summation of the total curvature including inclination and azimuth change in the planned well trajectory divided by the well depth. Secondly, the large scale tortuosity is the summation of the total curvature (inclination and azimuth changes) when a drilled well is measured while drilling (MWD) survey in local dogleg severity and then subtracted by the planned tortuosity ($T_p$). The micro-tortuosity is the tortuosity that occurs in the wellbore that is smaller in comparison to previous tortuosity. The total tortuosity can be calculated as:

$$T_{total} = T_p + T_l + T_m \tag{2.9}$$

Micro-tortuosity causes the spiral effect (Figure 2.15) when drilling tools run into the wellbore with the rotary assembly, and motor assembly and rotary assembly systems will cause poor hole quality. Spiraling can be easily eliminated. It is desirable to reduce micro-tortuosity to improve hole quality. It will be useful if T&D software programs also consider reducing this effect.

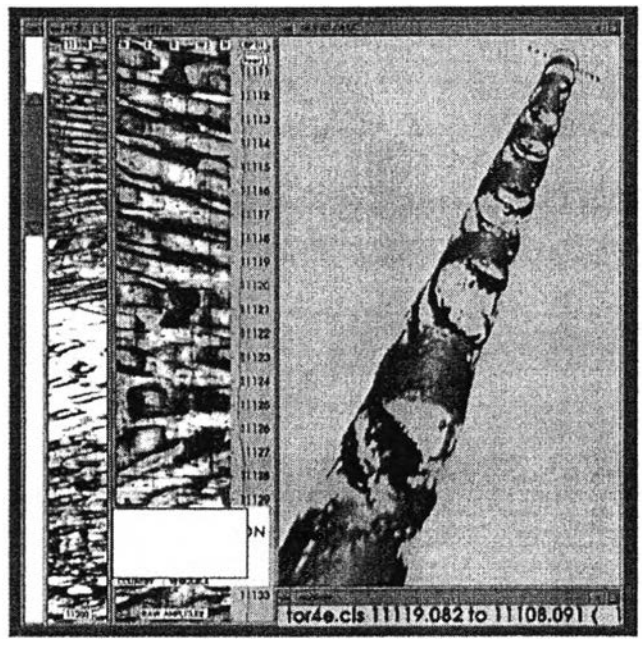


**Figure 2.15** Spiral borehole in 2D (Tracks 1 and 2) and 3D images (Gaynor *et al.*, 2001).

Gaynor *et al.* (2002) provided a mathematical model of a spiral hole and changed in diameter in torque equations which changed the diameter of tool joint ($D_{tj}$) to the average diameter ($D_{drift}$) as shown in Figure 2.16.

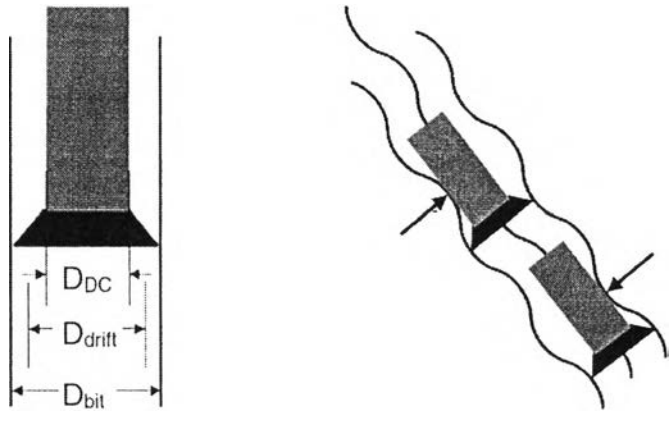


**Figure 2.16** The two-dimensional schematic of the drift equation (Gaynor *et al.*, 2001).

2.4.4 Buckling

Axial compression of drillstring will eventually lead to lateral deflection. The drillstring in compression will at first go into buckling called sinusoidal (Figure 2.17a), where the pipe goes from side to side in a snaky manner. When the drill pipe axial compressive load is increased further, the pipe will go into helical buckling (Figure 2.17b), where the drill pipe locks up in a spiraling manner against the sides of the borehole. The onset of buckling will depend on the stiffness of the string components and the outer diameter of components in relation to wellbore and casing. This is important for the torque and drag modeling since the helical buckling will cause a great increase in the side force between pipe and wellbore walls. The axial loading of pipes is a problem almost unique to the oil industry. Many equations have been derived for calculating the onset of sinusoidal and helical buckling (Tveitdal, 2011).

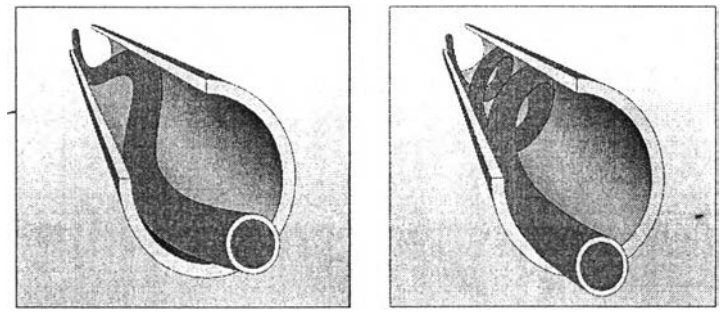

(a) (b)

**Figure 2.17** Buckling: (a) sinusoidal buckling and (b) helical buckling (Bennetzen *et al.*, 2010).

A long pipe in a wellbore will be buckled into a sinusoid along the lower side of the hole at an axial compressive force calculated as (Wu and Juvkam-Wold, 1993):

$$F_s = 2\sqrt{\frac{EIW_e}{r_c}\sin\theta} \qquad (2.10)$$

Where:

$F_s$ = the axial compressive force

EI = the stiffness of the pipe

$W_e$ = the buoyed linear weight of the pipe

$\theta$ = the inclination of the wellbore

$r_c$ = the radial clearance between the pipe and the wellbore

A helical buckling mode will not occur until the axial force ($F_H$) is

$$F_H = \sqrt{2}F_s \tag{2.11}$$

Buckling may then be assessed by calculating the friction force and using case selection below to define (Wu and Juvkam-Wold, 1993)

$F < F_s$ no buckling (2.12)

$F_s < F < \sqrt{2}F_s$ sinusoidal buckling initiated (2.13)

$\sqrt{2}F_s < F < (2\sqrt{2} - 1)F_s$ helical buckling initiated (2.14)

$(2\sqrt{2} - 1)F_s < F$ helical buckling (2.15)

## 2.5 Torque and Drag Equation in Three-Dimensional Wellbore

Prurapark (2009) developed a model for torque and drag calculations in three-dimension. It was developed based on a soft string model including the tortuousity effect and ignored any tubular stiffness effects. This means that the pipe is a heavy cable lying along the wellbore in different well geometry (Figure 2.18). This expresses that the axial tension and the torque forces are along the drillstring as well as the normal contact forces are supported by the wellbore. The derived equations define the axial force for tripping in, tripping out, and hoisting operations and also the torque for rotating on and off bottom of a string in the wellbore. In the operation modes, there are rotating off the bottom (RoffB), rotating on the bottom (RonB), pulling out of the hole (POOH), and running in the hole (RIH).

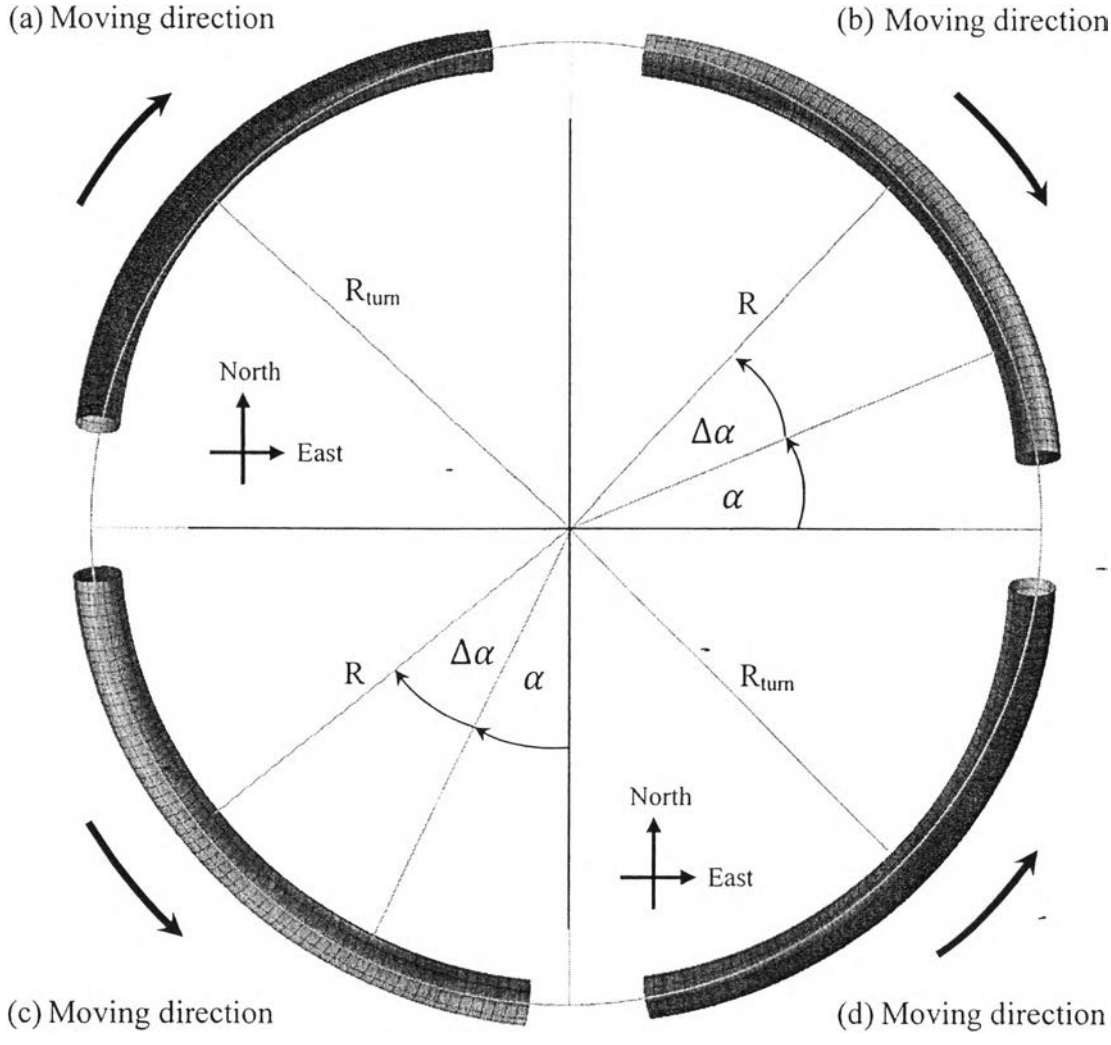


**Figure 2.18** Well geometry: (a) right turn (horizontal view), (b) drop-off section (vertical view), (c) build-up section (vertical view), and (d) left turn (horizontal view) (Aadnoy and Djurhuus, 2008).

2.5.1 Rotating Off Bottom (RoffB)

In this operation, the drillpipe is rotated by the top drive on the rig floor while the bit is not attached with the formation at the bottom. Most cases is aim to release the make-up torque from the top drive. Different well sections experience with discrepancy of torque and drag equations can be expressed below.

*2.5.1.1 Build Section*

Normal contact force in build section (Figure 2.19) can be calculated as:

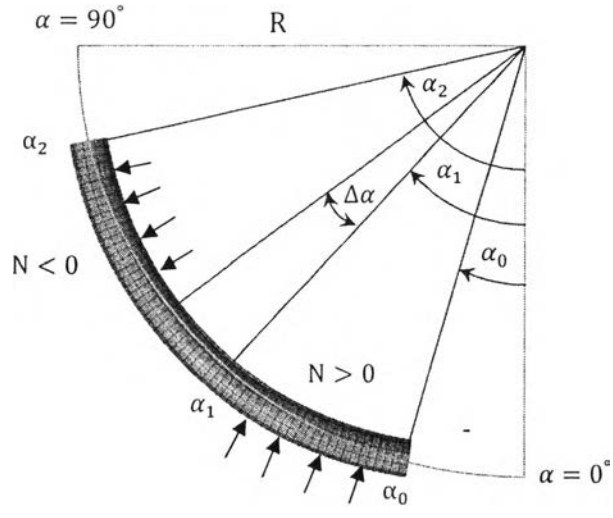


**Figure 2.19** Illustration of differences between positive (downside) and negative (upside) normal contact forces in build section during RoffB (Prurapark, 2009).

$$N = W_e cos(\alpha) - \frac{F(\alpha)}{R} \tag{2.16}$$

Axial force in build section (Figure 2.20) can be calculated as:

$$\frac{d(F)}{d(\alpha)} = W_e R sin(\alpha) \tag{2.17}$$

Torque in build section can be calculated as:

$$T(\alpha_2) = \int_{\alpha_0}^{\alpha_1} \mu \left\{ \sqrt{\left[W_e cos(\alpha) - \frac{F(\alpha)}{R}\right]^2 + \left[\frac{F(\alpha)}{R_{turn}}\right]^2} \right\} \frac{D_{drift}}{24} R d\alpha + \int_{\alpha_1}^{\alpha_2} -\mu \left\{ \sqrt{\left[W_e cos(\alpha) - \frac{F(\alpha)}{R}\right]^2 + \left[\frac{F(\alpha)}{R_{turn}}\right]^2} \right\} \frac{D_{drift}}{24} R d\alpha \tag{2.18}$$

*2.5.1.2 Hold Section*

Normal contact force in hold section (Figure 2.21) can be calculated as:

$$N = W_e sin(I) \tag{2.19}$$

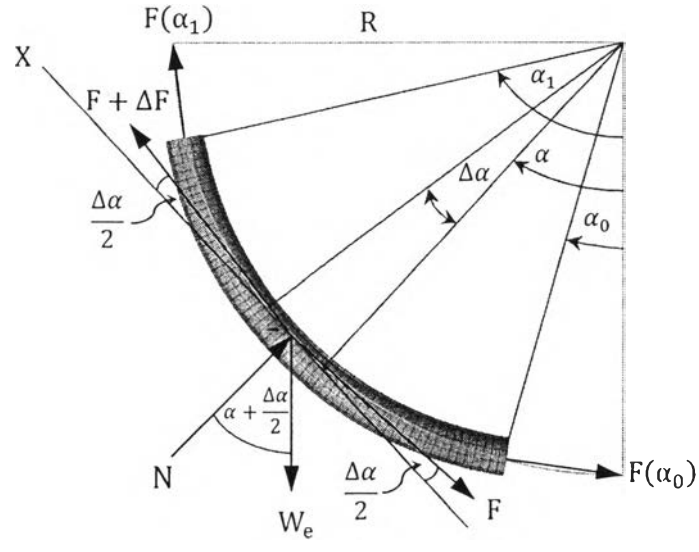


**Figure 2.20** Illustration of forces (axial force, F and normal contact force, N) in build section during RoffB (Prurapark, 2009).

Axial force in hold section (Figure 2.21) can be calculated as:

$$\Delta F = W_e cos(I) \tag{2.20}$$

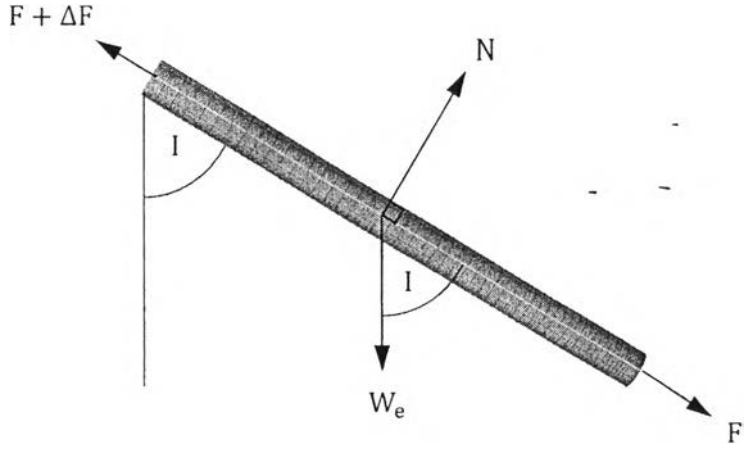


**Figure 2.21** Illustration of forces (axial force, F and normal contact force, N) in hold section during RoffB (Prurapark, 2009).

Torque in build section can be calculated as:

$$T(L_1) = \int_{L_0}^{L_1} \mu \left\{ \sqrt{[W_e sin(I)]^2 + \left[\frac{F(L)}{R_{turn}}\right]^2} \right\} \frac{D_{drift}}{24} RdL \qquad (2.21)$$

*2.5.1.3 Drop Section*

Normal contact force in drop section (Figure 2.22) can be calculated as:

$$N = W_e sin(\alpha) + \frac{F(\alpha)}{R} \qquad (2.22)$$

Axial force in drop section (Figure 2.23) can be calculated as:

$$\frac{d(F)}{d(\alpha)} = W_e R cos(\alpha) \qquad (2.23)$$

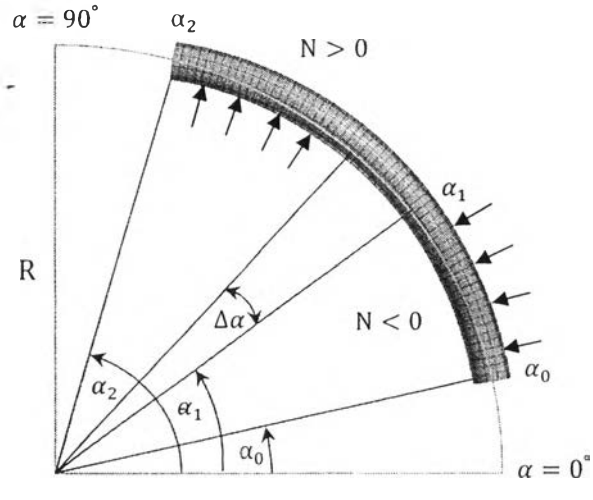


**Figure 2.22** Illustration of differences between positive (downside) and negative (upside) normal contact forces in drop section during RoffB (Prurapark, 2009).

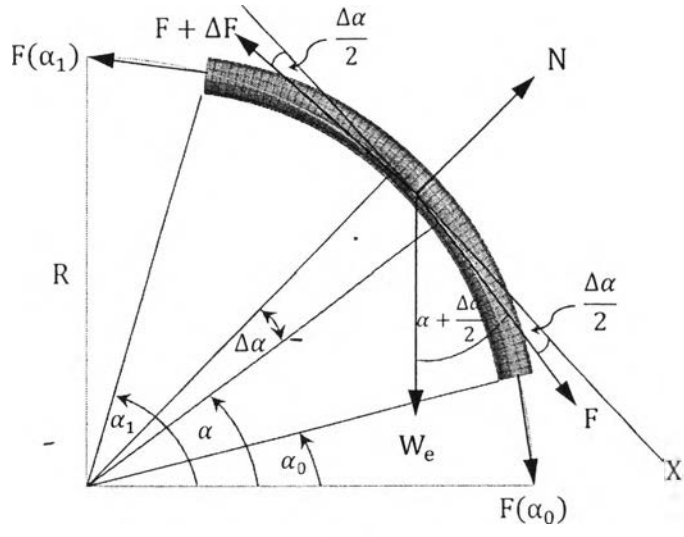


**Figure 2.23** Illustration of forces (axial force, F and normal contact force, N) in drop section during RoffB (Prurapark, 2009).

Torque in drop section can be calculated as:

$$T(\alpha_2) = \int_{\alpha_0}^{\alpha_1} \mu \left\{ \sqrt{\left[W_e sin(\alpha) + \frac{F(\alpha)}{R}\right]^2 + \left[\frac{F(\alpha)}{R_{turn}}\right]^2} \right\} \frac{D_{drift}}{24} R d\alpha + \int_{\alpha_1}^{\alpha_2} -\mu \left\{ \sqrt{\left[W_e sin(\alpha) + \frac{F(\alpha)}{R}\right]^2 + \left[\frac{F(\alpha)}{R_{turn}}\right]^2} \right\} \frac{D_{drift}}{24} R d\alpha \quad (2.24)$$

*2.5.1.4 Left right turn*

Normal contact force while the wellbore turns right (Figure 2.24) can be calculated as:

$$N_{turn} = \frac{F(\alpha)}{R_{turn}} \quad (2.25)$$

Normal contact force while the wellbore turns left (Figure 2.25) can be calculated as:

$$N_{turn} = \frac{F(\alpha)}{R_{turn}} \quad (2.26)$$

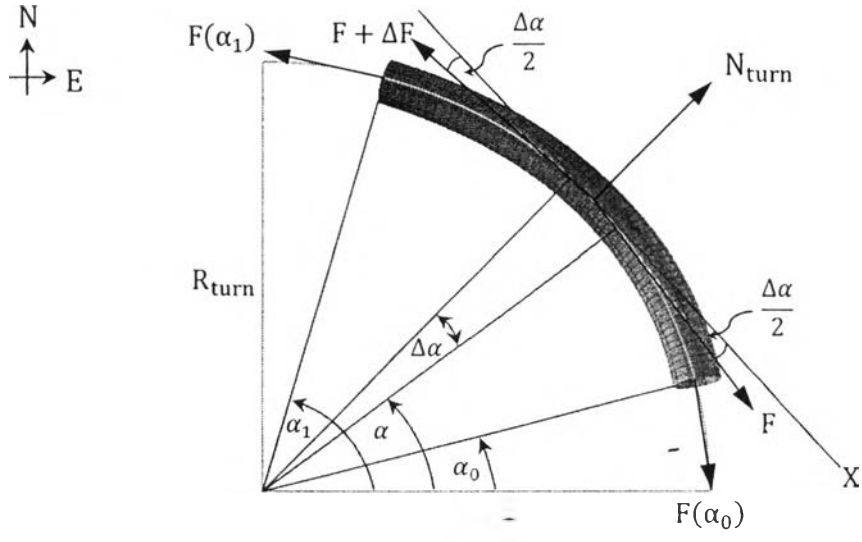


**Figure 2.24** Illustration of forces (axial force, F and normal contact force, N) when the wellbore turns right (horizontal view) during RoffB (Prurapark, 2009).

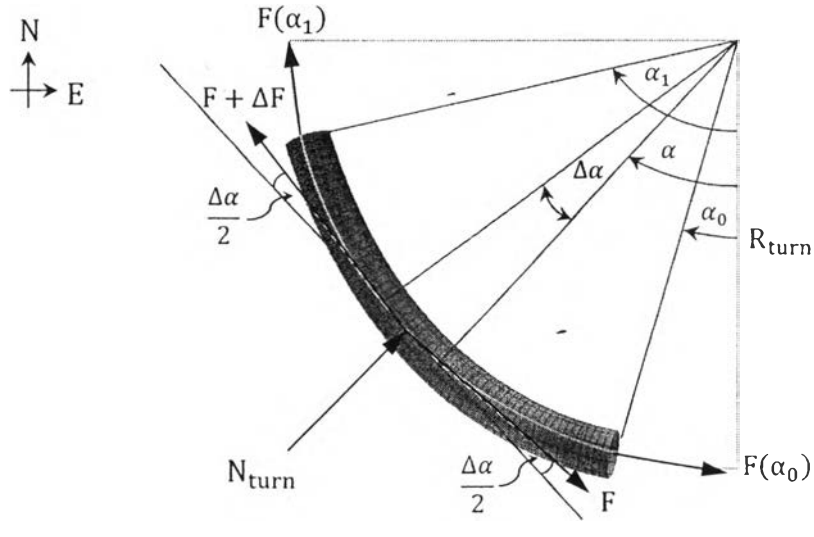


**Figure 2.25** Illustration of forces (axial force, F and normal contact force, N) when the wellbore turns left (horizontal view) during RoffB (Prurapark, 2009).

2.5.2 Pulling Out of the Hole (POOH)

This operation normally occurs in drilling process. The drillpipe is pull by the cable on the rig floor while the drillstring experience with the formation

along the wellbore creating a resistance to move axially. Different well types experience with discrepancy of torque and drag equations expressed below.

*2.5.2.1 Build Section*

Normal contact force in build section (Figure 2.26) can be calculated as:

$$N = W_e cos(\alpha) - \frac{F(\alpha)}{R} \quad (2.27)$$

Axial force in build section (Figure 2.27) can be calculated as:

For $N > 0$ and $(\alpha_1 \geq \alpha \geq \alpha_0)$

$$\frac{d(F)}{d(\alpha)} = \mu \left\{ \sqrt{\left[W_e cos(\alpha) - \frac{F(\alpha)}{R}\right]^2 + \left[\frac{F(\alpha)}{R_{turn}}\right]^2} \right\} R + W_e R sin(\alpha) \quad (2.28a)$$

For $N < 0$ and $(\alpha_2 \geq \alpha \geq \alpha_1)$

$$\frac{d(F)}{d(\alpha)} = \mu \left\{ -\sqrt{\left[W_e cos(\alpha) - \frac{F(\alpha)}{R}\right]^2 + \left[\frac{F(\alpha)}{R_{turn}}\right]^2} \right\} R + W_e R sin(\tilde{\alpha}) \quad (2.28b)$$

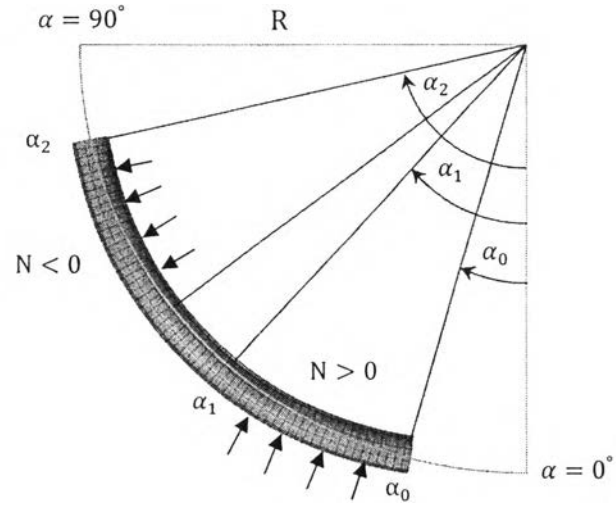


**Figure 2.26** Illustration of differences between positive (downside) and negative (upside) normal contact forces in build section during POOH (Prurapark, 2009).

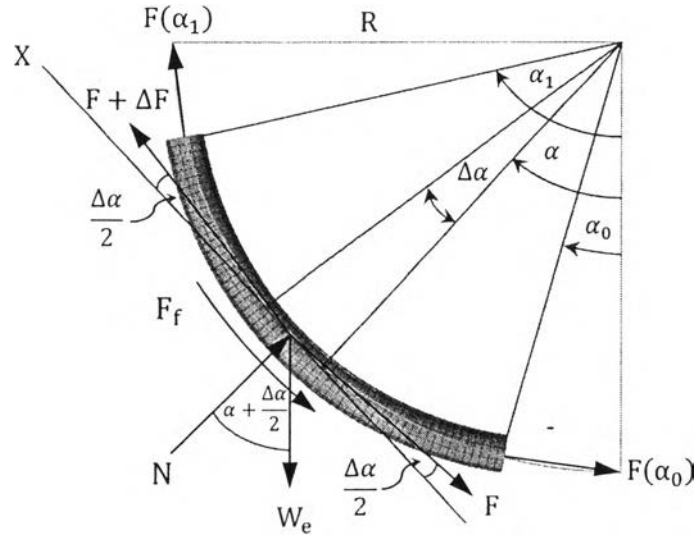


**Figure 2.27** Illustration of forces (axial force, F and normal contact force, N) in build section during POOH (Prurapark, 2009).

*2.5.2.2 Hold Section*

Normal contact force in hold section (Figure 2.28) can be calculated as:

$$N = W_e sin(I) \tag{2.29}$$

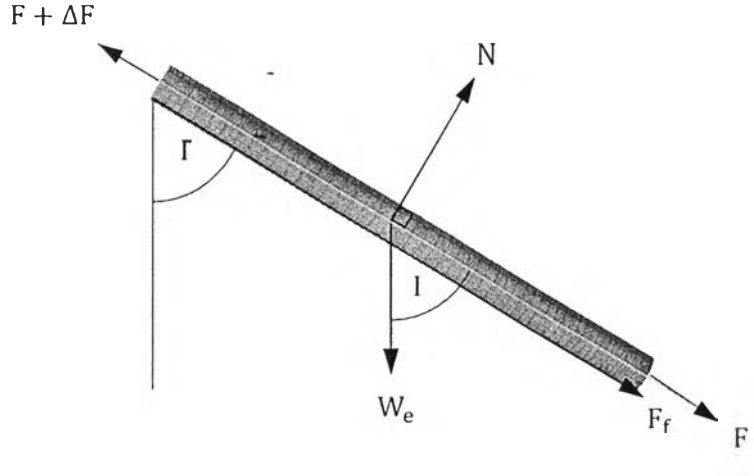


**Figure 2.28** Illustration of forces (axial force, F and normal contact force, N) in hold section during POOH (Prurapark, 2009).

Axial force in hold section (Figure 2.28) can be calculated as:

$$\Delta F = \mu N_{total} + W_e cos(I) \quad (2.30)$$

*2.5.2.3 Drop Section*

Normal contact force in drop section (Figure 2.29) can be calculated as:

$$N = W_e sin(\alpha) + \frac{F(\alpha)}{R} \quad (2.31)$$

Axial force in drop section (Figure 2.30) can be calculated as:

For N > 0 and ($\alpha_1 \geq \alpha \geq \alpha_0$ )

$$\frac{d(F)}{d(\alpha)} = \mu \left\{ \sqrt{\left[W_e sin(\alpha) + \frac{F(\alpha)}{R}\right]^2 + \left[\frac{F(\alpha)}{R_{turn}}\right]^2} \right\} R + W_e R cos(\alpha) \quad (2.32a)$$

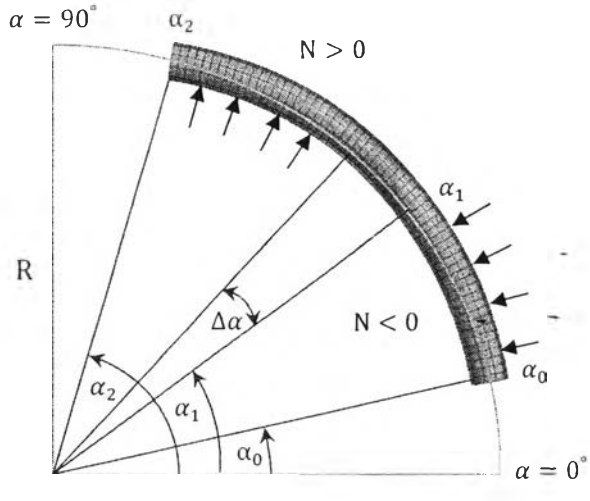


**Figure 2.29** Illustration of differences between positive (downside) and negative (upside) normal contact forces in drop section during POOH (Prurapark, 2009).

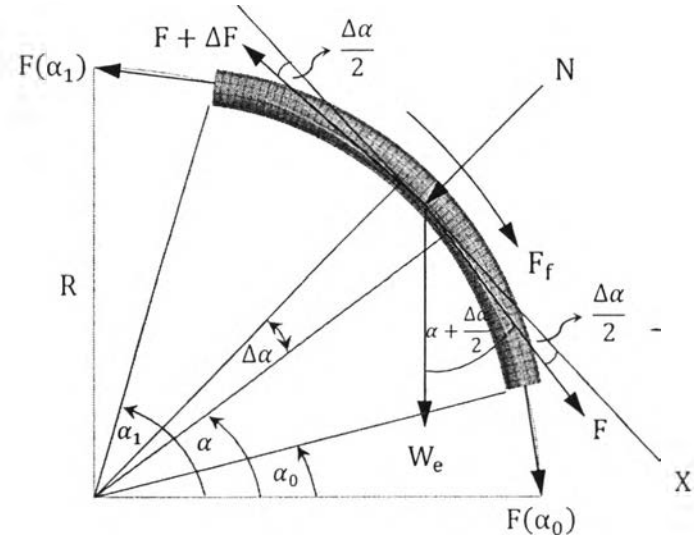


**Figure 2.30** Illustration of forces (axial force, F and normal contact force, N) in drop section during POOH (Prurapark, 2009).

For $N < 0$ and $(\alpha_2 \geq \alpha \geq \alpha_1)$

$$\frac{d(F)}{d(\alpha)} = \mu\left\{-\sqrt{\left[W_e sin(\alpha) + \frac{F(\alpha)}{R}\right]^2 + \left[\frac{F(\alpha)}{R_{turn}}\right]^2}\right\} R + W_e R cos(\alpha) \quad (2.32b)$$

*2.5.2.4 Left right turn*

Normal contact force while the wellbore turns right (Figure 2.31) can be calculated as:

$$N_{turn} = \frac{F(\alpha)}{R_{turn}} \quad (2.33)$$

Normal contact force while the wellbore turns left (Figure 2.32) can be calculated as:

$$N_{turn} = \frac{F(\alpha)}{R_{turn}} \quad (2.34)$$

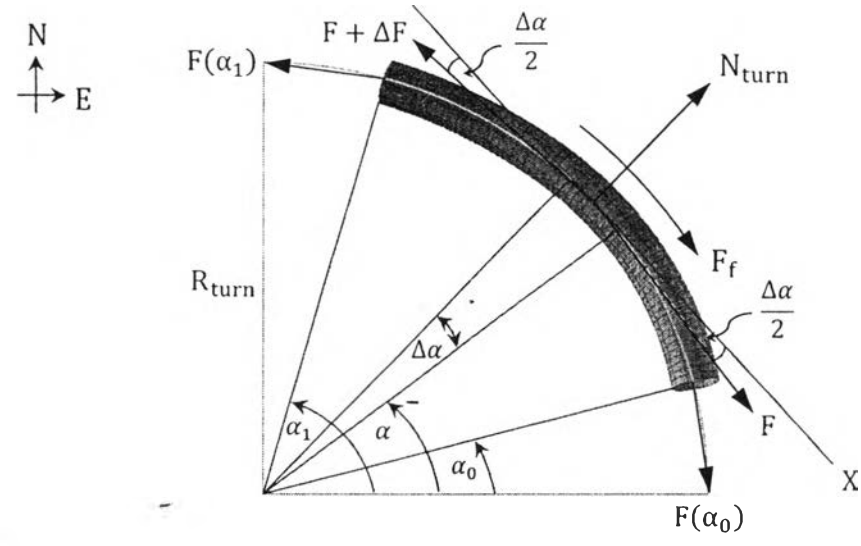


**Figure 2.31** Illustration of forces (axial force, F and normal contact force, N) when the wellbore turns right (horizontal view) during POOH (Prurapark, 2009).

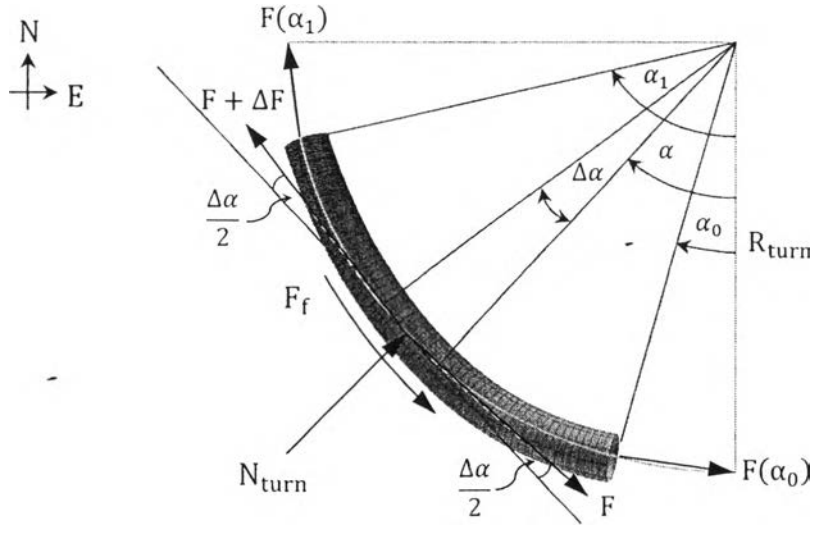


**Figure 2.32** Illustration of forces (axial force, F and normal contact force, N) when the wellbore turns left (horizontal view) during POOH (Prurapark, 2009).

2.5.3 Running into the Hole (RIH)

This operation generally takes place when extends the drillpipe to reach the target. The drillpipe is push by the cable, however the drillstring also experience with the formation along the wellbore creating a resistance to move

axially. Different well types experience with discrepancy of torque and drag equations expressed below.

*2.5.3.1 Build Section*

Normal contact force in build section (Figure 2.33) can be calculated as:

$$N = W_e cos(\alpha) + \frac{F_c(\alpha)}{R} \qquad (2.35)$$

Axial force in build section (Figure 2.34) can be calculated as:

For N > 0 and ($\alpha_1 \geq \alpha \geq \alpha_0$ )

$$\frac{d(F)}{d(\alpha)} = \mu\left\{\sqrt{\left[W_e cos(\alpha) + \frac{F_c(\alpha)}{R}\right]^2 + \left[\frac{F_c(\alpha)}{R_{turn}}\right]^2}\right\}R - W_e R sin(\alpha) \qquad (2.36a)$$

For N < 0 and ($\alpha_2 \geq \alpha \geq \alpha_1$ )

$$\frac{d(F)}{d(\alpha)} = \mu\left\{-\sqrt{\left[W_e cos(\alpha) + \frac{F_c(\alpha)}{R}\right]^2 + \left[\frac{F_c(\alpha)}{R_{turn}}\right]^2}\right\}R - W_e R sin(\alpha) \qquad (2.36b)$$

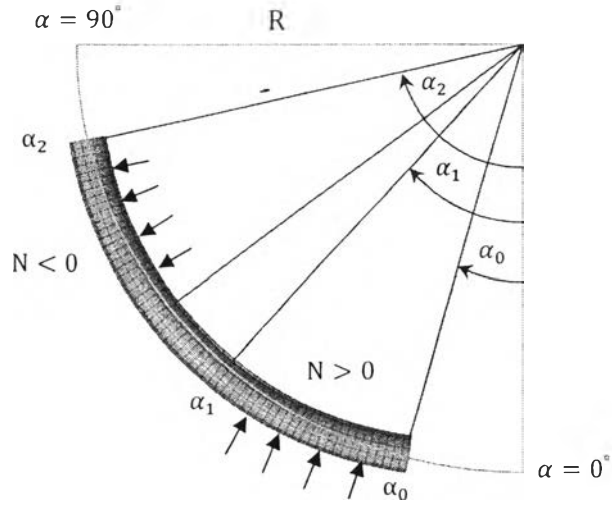


**Figure 2.33** Illustration of differences between positive (downside) and negative (upside) normal contact forces in build section during RIH (Prurapark, 2009).

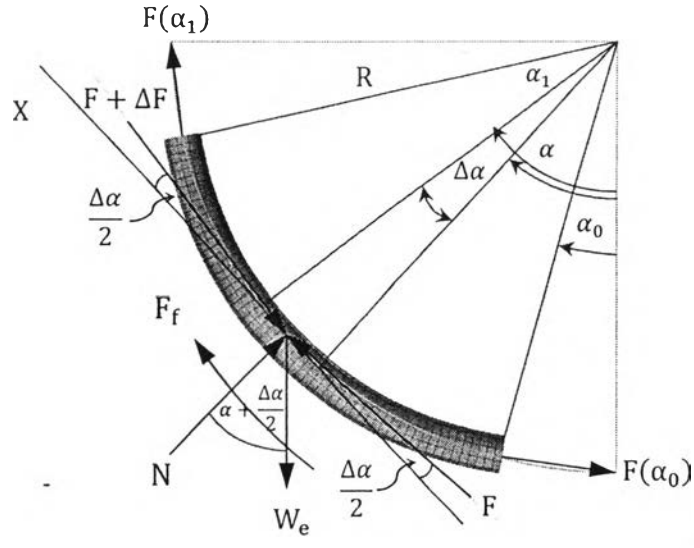


**Figure 2.34** Illustration of forces (axial force, F and normal contact force, N) in build section during RIH (Prurapark, 2009).

*2.5.3.2 Hold Section*

Normal contact force in hold section (Figure 2.35) can be calculated as:

$$N = W_e sin(I) \tag{2.37}$$

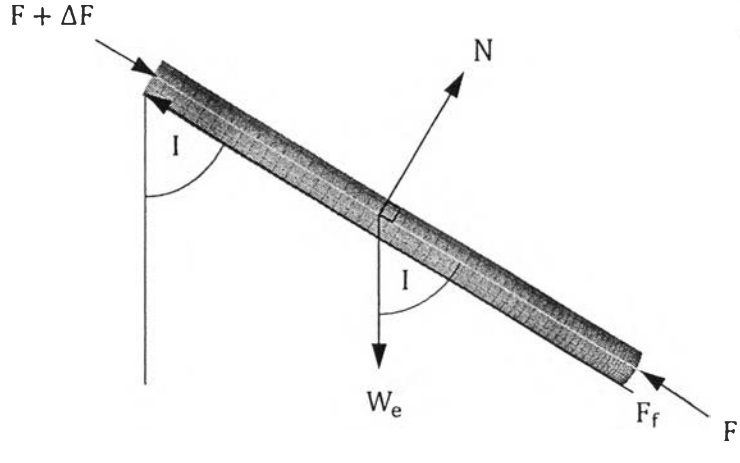


**Figure 2.35** Illustration of forces (axial force, F and normal contact force, N) in hold section during RIH (Prurapark, 2009).

*2.5.3.3 Drop Section*

Normal contact force in drop section (Figure 2.36) can be calculated as:

$$N = W_e sin(\alpha) - \frac{F_c(\alpha)}{R} \quad (2.39)$$

Axial force in drop section (Figure 2.37) can be calculated as:

For N > 0 and ($\alpha_1 \geq \alpha \geq \alpha_0$)

$$\frac{d(F)}{d(\alpha)} = \mu\left\{\sqrt{\left[W_e sin(\alpha) - \frac{F_c(\alpha)}{R}\right]^2 + \left[\frac{F_c(\alpha)}{R_{turn}}\right]^2}\right\} R - W_e R cos(\alpha) \quad (2.40a)$$

For N < 0 and ($\alpha_2 \geq \alpha \geq \alpha_1$)

$$\frac{d(F)}{d(\alpha)} = \mu\left\{-\sqrt{\left[W_e sin(\alpha) - \frac{F_c(\alpha)}{R}\right]^2 + \left[\frac{F_c(\alpha)}{R_{turn}}\right]^2}\right\} R - W_e R cos(\alpha) \quad (2.40b)$$

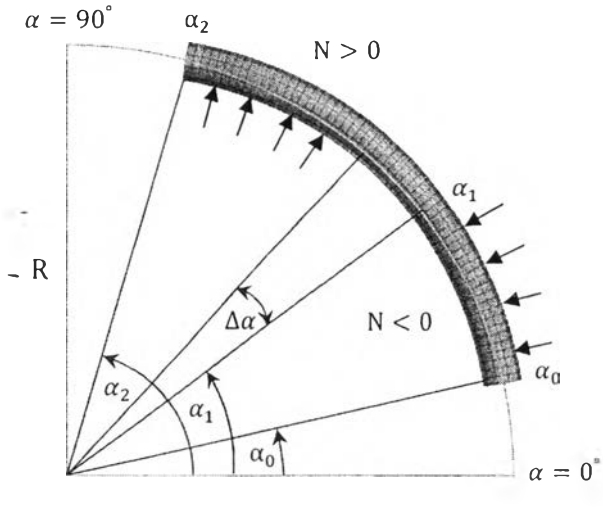


**Figure 2.36** Illustration of differences between positive (downside) and negative (upside) normal contact forces in drop section during RIH (Prurapark, 2009).

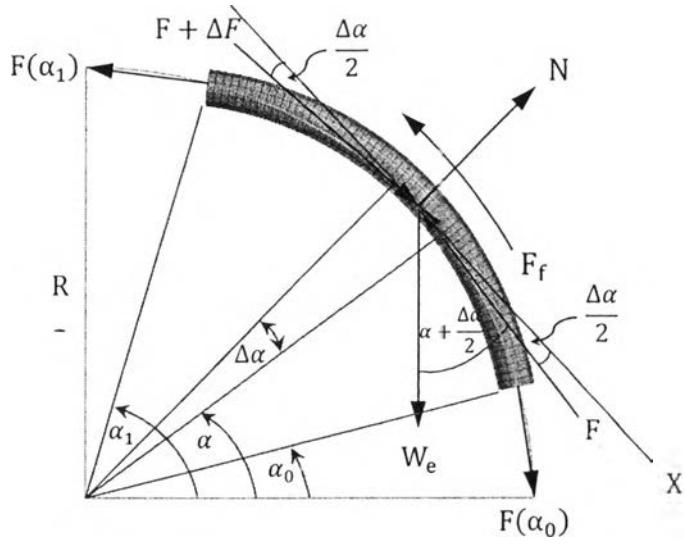


**Figure 2.37** Illustration of forces (axial force, F and normal contact force, N) in drop section during RIH (Prurapark, 2009).

*2.5.3.4 Left right turn*

Normal contact force while the wellbore turns right (Figure 2.38) can be calculated as:

$$N_{turn} = -\frac{F_c(\alpha)}{R_{turn}} \tag{2.41}$$

Normal contact force while the wellbore turns left (Figure 2.39) can be calculated as:

$$N_{turn} = \frac{F_c(\alpha)}{R_{turn}} \tag{2.42}$$

2.5.4 Rotating On Bottom (RonB)

The drillstring is rotated by the top drive on the rig floor cooperated with applying the weight to bit for penetrating the formation at the bottom. Different well types experience with discrepancy of torque and drag equations expressed below.

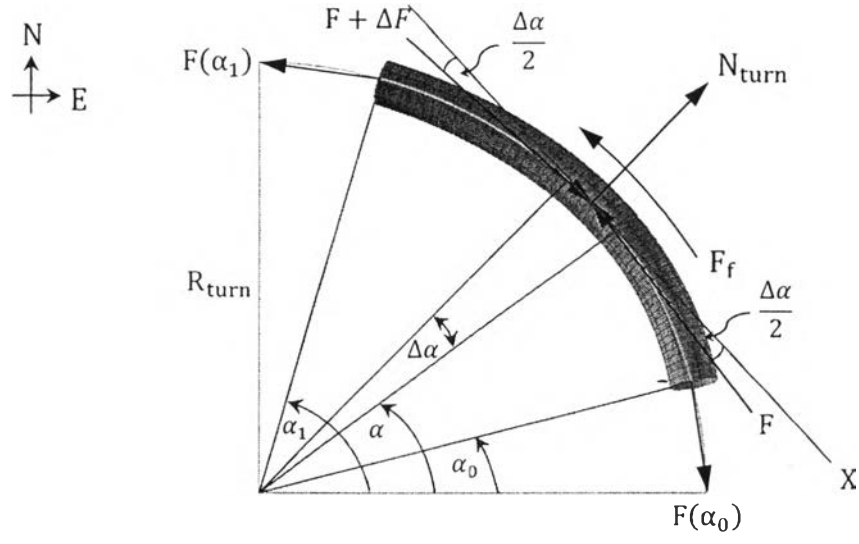


**Figure 2.38** Illustration of forces (axial force, F and normal contact force, N) when the wellbore turns right (horizontal view) during RIH (Prurapark, 2009).

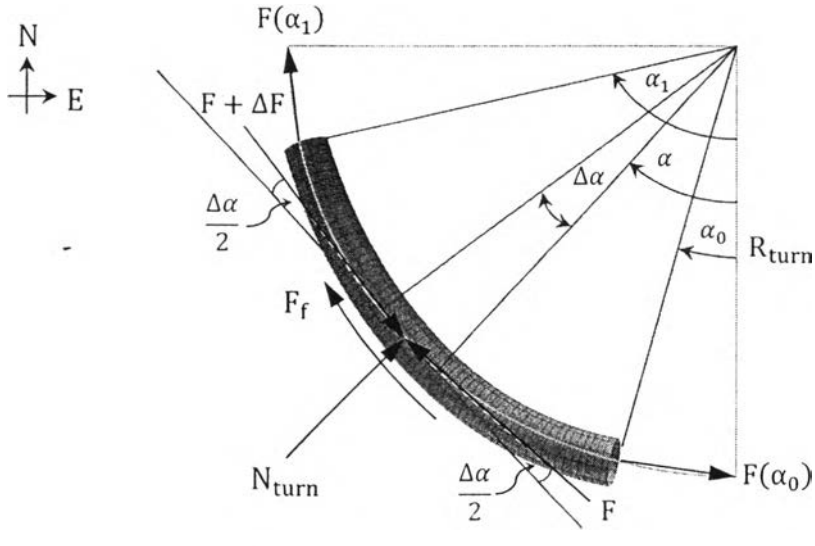


**Figure 2.39** Illustration of forces (axial force, F and normal contact force, N) when the wellbore turns left (horizontal view) during RIH (Prurapark, 2009).

*2.5.4.1 Build Section*

Normal contact force in build section (Figure 2.40) can be calculated as:

$$N = W_e cos(\alpha) + \frac{F_c(\alpha)}{R} \quad (2.43)$$

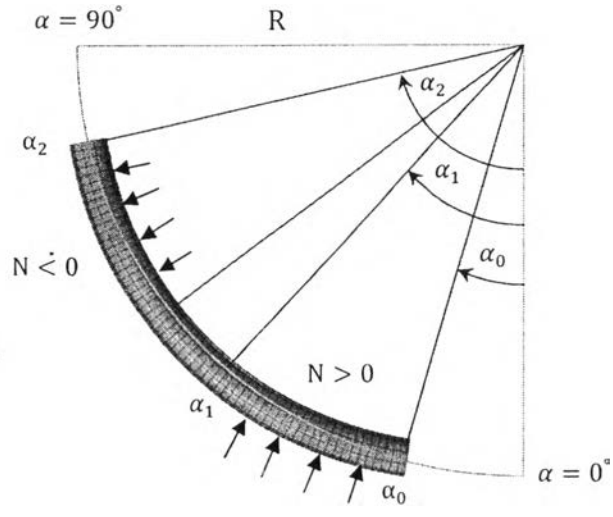


**Figure 2.40** Illustration of differences between positive (downside) and negative (upside) normal contact forces in build section during RonB (Prurapark, 2009).

Axial force in build section (Figure 2.41) can be calculated as:

For $N > 0$ and $(\alpha_1 \geq \alpha \geq \alpha_0)$

$$\frac{d(F)}{d(\alpha)} = \mu\left\{\sqrt{\left[W_e cos(\alpha) + \frac{F_c(\alpha)}{R}\right]^2 + \left[\frac{F_c(\alpha)}{R_{turn}}\right]^2}\right\}R - W_e R sin(\alpha) \quad (2.44a)$$

For $N < 0$ and $(\alpha_2 \geq \alpha \geq \alpha_1)$

$$\frac{d(F)}{d(\alpha)} = \mu\left\{-\sqrt{\left[W_e cos(\alpha) + \frac{F_c(\alpha)}{R}\right]^2 + \left[\frac{F_c(\alpha)}{R_{turn}}\right]^2}\right\}R - W_e R sin(\alpha) \quad (2.44b)$$

Torque in build section can be calculated as:

$$T(\alpha_2) = \int_{\alpha_0}^{\alpha_1} \mu\left\{\sqrt{\left[W_e cos(\alpha) + \frac{F_c(\alpha)}{R}\right]^2 + \left[\frac{F_c(\alpha)}{R_{turn}}\right]^2}\right\}\frac{D_{drift}}{24} R d\alpha + \int_{\alpha_1}^{\alpha_2} -\mu\left\{\sqrt{\left[W_e cos(\alpha) + \frac{F_c(\alpha)}{R}\right]^2 + \left[\frac{F_c(\alpha)}{R_{turn}}\right]^2}\right\}\frac{D_{drift}}{24} R d\alpha \quad (2.45)$$

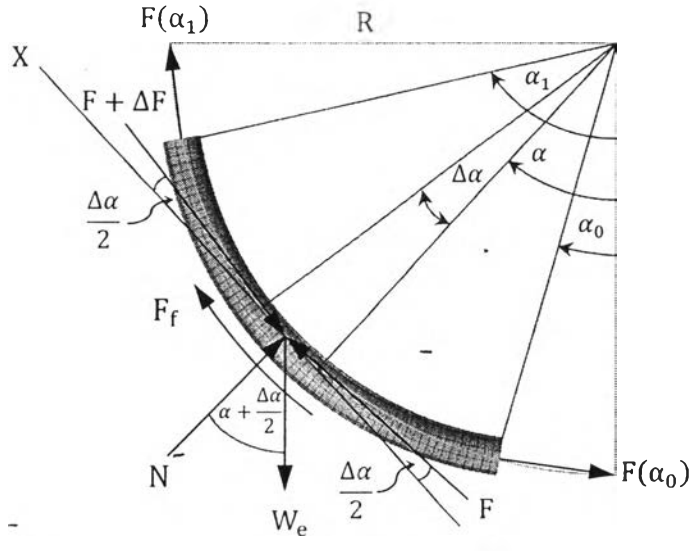


**Figure 2.41** Illustration of forces (axial force, F and normal contact force, N) in build section during RonB (Prurapark, 2009).

*2.5.4.2 Hold Section*

Normal contact force in hold section (Figure 2.42) can be calculated as:

$$N = W_e sin(I) \tag{2.46}$$

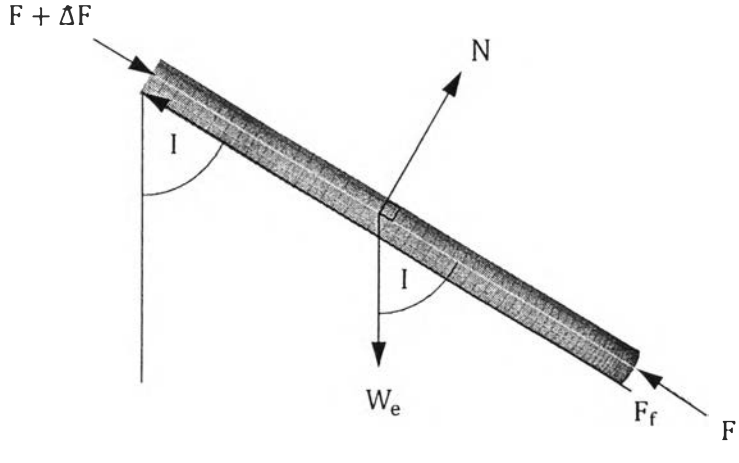


**Figure 2.42** Illustration of forces (axial force, F and normal contact force, N) in hold section during RonB (Prurapark, 2009).

Axial force in hold section (Figure 2.42) can be calculated as:

$$\Delta F = \mu N_{total} - W_e cos(I) \tag{2.47}$$

Torque in hold section can be calculated as:

$$T(L_1) = \int_{L_0}^{L_1} \mu \left\{ \sqrt{[W_e sin(I)]^2 + \left[\frac{F_c(L)}{R_{turn}}\right]^2} \right\} \frac{D_{drift}}{24} R dL \tag{2.48}$$

*2.5.4.3 Drop Section*

Normal contact force in drop section (Figure 2.43) can be calculated as:

$$N = W_e sin(\alpha) - \frac{F_c(\alpha)}{R} \tag{2.49}$$

Axial force in drop section (Figure 2.44) can be calculated as:

For $N > 0$ and $(\alpha_1 \geq \alpha \geq \alpha_0)$

$$\frac{d(F)}{d(\alpha)} = \mu \left\{ \sqrt{\left[W_e sin(\alpha) - \frac{F_c(\alpha)}{R}\right]^2 + \left[\frac{F_c(\alpha)}{R_{turn}}\right]^2} \right\} R - W_e R cos(\alpha) \tag{2.50a}$$

For $N < 0$ and $(\alpha_2 \geq \alpha \geq \alpha_1)$

$$\frac{d(F)}{d(\alpha)} = \mu \left\{ -\sqrt{\left[W_e sin(\alpha) - \frac{F_c(\alpha)}{R}\right]^2 + \left[\frac{F_c(\alpha)}{R_{turn}}\right]^2} \right\} R - W_e R cos(\alpha) \tag{2.50b}$$

Torque in drop section can be calculated as:

$$T(\alpha_2) = \int_{\alpha_0}^{\alpha_1} \mu \left\{ \sqrt{\left[W_e sin(\alpha) - \frac{F_c(\alpha)}{R}\right]^2 + \left[\frac{F_c(\alpha)}{R_{turn}}\right]^2} \right\} \frac{D_{drift}}{24} R d\alpha + \int_{\alpha_1}^{\alpha_2} -\mu \left\{ \sqrt{\left[W_e sin(\alpha) - \frac{F_c(\alpha)}{R}\right]^2 + \left[\frac{F_c(\alpha)}{R_{turn}}\right]^2} \right\} \frac{D_{drift}}{24} R d\alpha \tag{2.51}$$

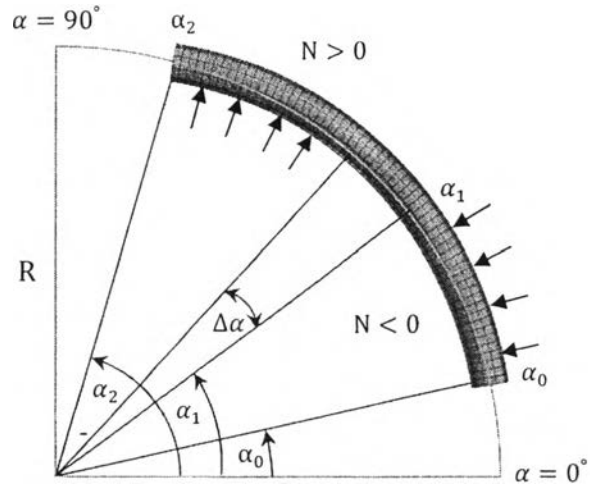


**Figure 2.43** Illustration of differences between positive (downside) and negative (upside) normal contact forces in drop section during RonB (Prurapark, 2009).

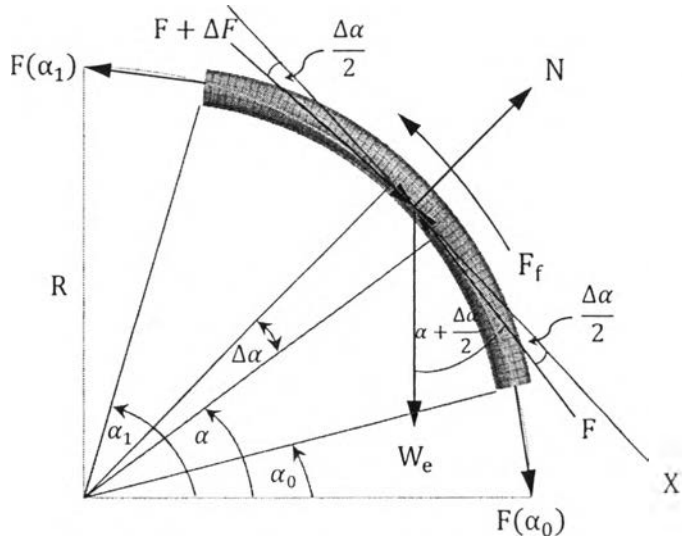


**Figure 2.44** Illustration of forces (axial force, F and normal contact force, N) in drop section during RonB (Prurapark, 2009).

*2.5.4.4 Left right turn*

Normal contact force while the wellbore turns right (Figure 2.45) can be calculated as:

$$N_{turn} = -\frac{F_c(\alpha)}{R_{turn}} \tag{2.52}$$

Normal contact force while the wellbore turns left (Figure 2.46) can be calculated as:

$$N_{turn} = \frac{F_c(\alpha)}{R_{turn}} \tag{2.53}$$

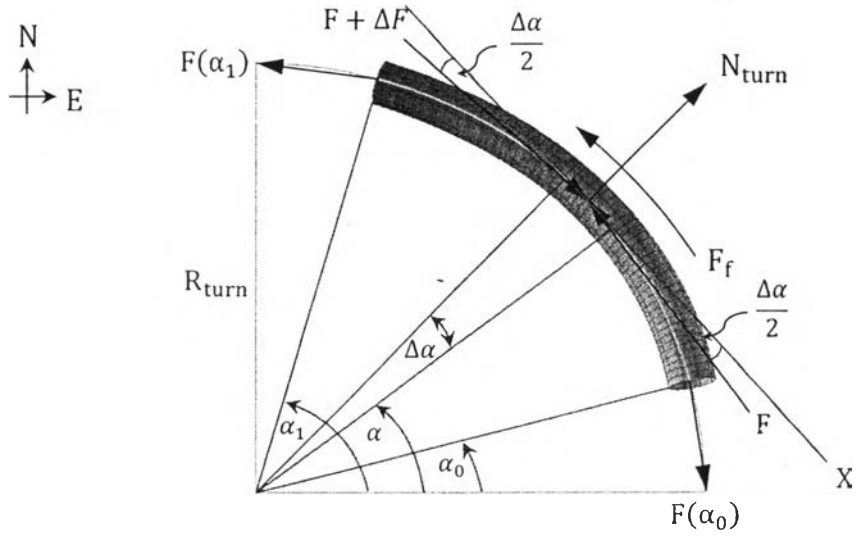


**Figure 2.45** Illustration of forces (axial force, F and normal contact force, N) when the wellbore turns right (horizontal view) during RonB (Prurapark, 2009).

## 2.6 Software Development

Well planning is usually an iterative process to determine the optimal balance among wellpath, fluid and hydraulic requirements, drillstring design, torque & drag, casing setting depth etc. The iterative process not only covers the wellpath design, but also the operations planning as well. There are many variables in designing a well, such as kick off point (KOP), dogleg severity (DLS), horizontal departure, etc., it becomes an iterative process aimed at yielding an optimal design which should result in the simplest path while still achieving all geological targets. In order to achieve an optimum well path, several factors have to be considered and put

into perspective. Based on reported industry experience gained from earlier wells and confirmed during the drilling of more recent wells, the following aspects are considered to be key factors in well planning (Agbaji, 2010). Figure 2.47 shows well planning process to develop drilling operation in order to represent a suitable plan to reach the objective.

The torque and drag is related to and affected by many things including the wellpath design, drillstring design, hole size, drilling fluid, etc. High levels of torque & drag can lead to situations where the casing, liner and/or completion cannot be installed at the planned depth. This module performs T&D analysis for the well design. Since there are many commercially available T&D analysis softwares, it is anticipated that one of these packages will be used. However, in addition to the inputs provided by commercially available software, this project calculates the torque generated at the bit, the surface torque, fracture gradient, fracture pressure, and maximum mud density. Figure 2.48 is the flowchart of the torque and drag analysis.

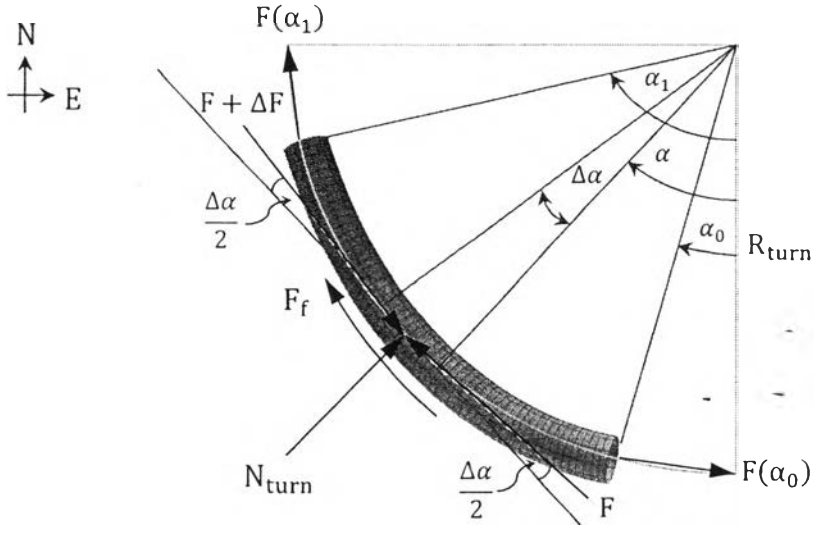


**Figure 2.46** Illustration of forces (axial force, F and normal contact force, N) when the wellbore turns left (horizontal view) during RonB (Prurapark, 2009).

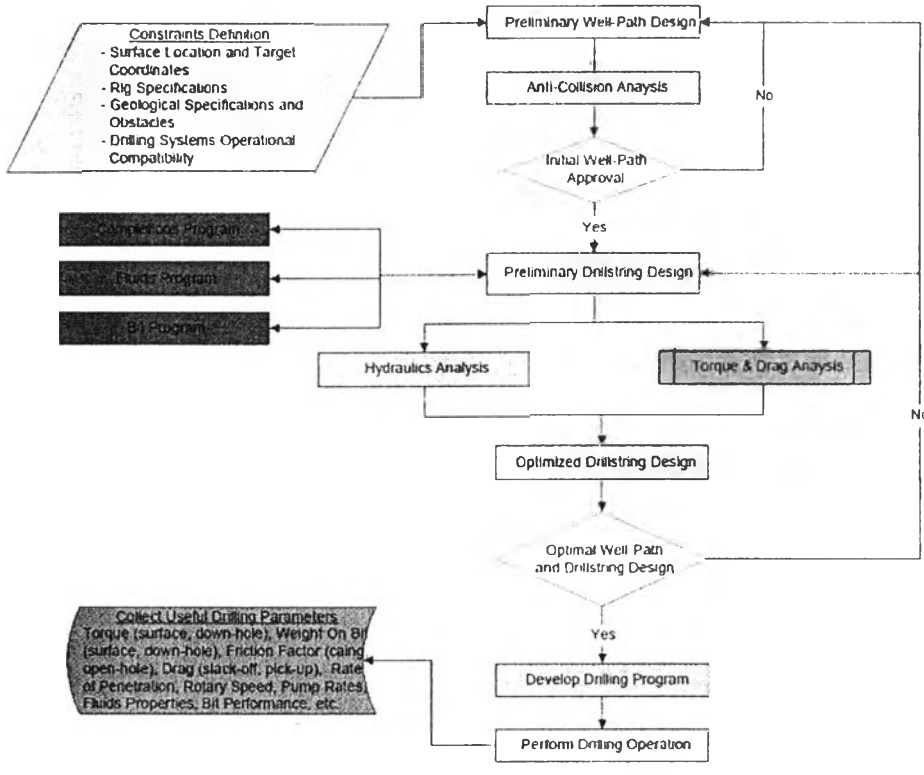


**Figure 2.47** Well planning and engineering flowchart (Adewuya and Pham, 1998).

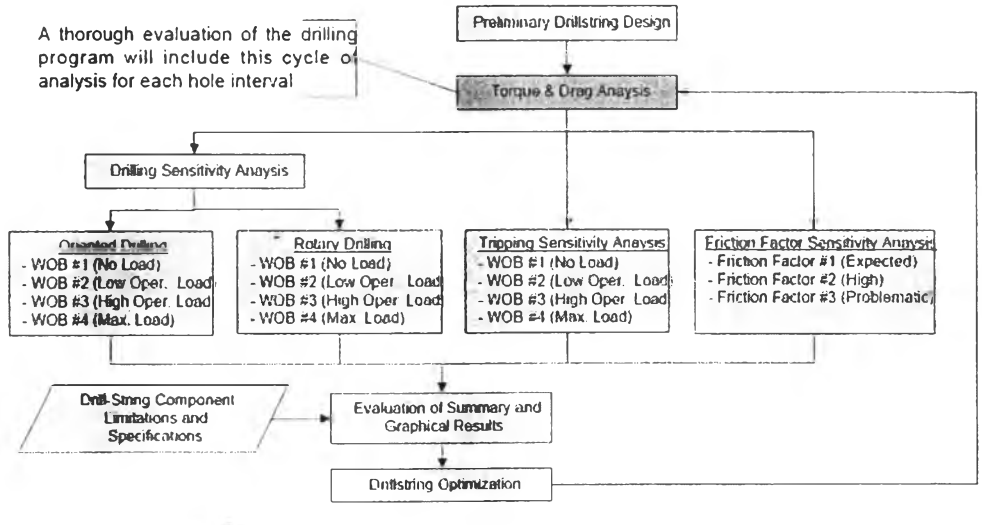


**Figure 2.48** Torque and drag analysis flowchart (Adewuya and Pham,. 1998).

## 2.7 Numerical Method

### 2.7.1 Euler Method

The Euler method is the most straightforward method to integrate a differential equation. The first-order differential equation is considered.

$$\frac{dy}{dx} = f(x, y) \tag{2.54}$$

A value of y for any given value of x is determined, that is $y = y_0$ at $x = 0$, a solution to the initial-value.

The derivative dy/dx is determined as a finite difference, $(y_{i+1} - y_i)/(x_{i+1} - x_i)$ and evaluated as the function at $[x_i, y_i]$ written as

$$y_{i+1} = y_i + \Delta x f(x, y) \tag{2.55}$$

where $\Delta x = x_{i+1} - x_i$. Equation (2.55) is known as the Euler method for solving a first-order ordinary differential equations (ODEs) numerically. Given an initial value for y ($y = y_0$ at $x = 0$) and a step size $\Delta x$, the equation is successively applied to find $y_1, y_2, y_3, \ldots, y_n$ at the corresponding values of $x_1, x_2, x_3, \ldots, x_4$.

### 2.7.2 Modified Euler Method or Euler Predictor-Corrector Method

In the Euler method, each value of y is estimated based on a linear extrapolation from the last computed value. The more nearly linear the function or the smaller the step size, the better this estimate is likely to be. This could improve the accuracy, if a better estimate of the average slope of the function is made over each interval stepping through the solution. If the value of $y'$ at x is known in advance, $x + \Delta x$ could be used and the mean of these slopes improve the estimate:

$$y_{i+1} = y_i + \Delta x \frac{y_i' + y_{i+1}'}{2} \tag{2.56}$$

However, the value of $y_{i+1}$ or $y'_{i+1}$ is not known in advance. Once $y_{i+1}$ is computed using the Euler method (Figure 2.49), the computed value is used to estimate $y'_{i+1}$ which is then used to get an improved or "corrected" value of $y_{i+1}$. The difference between the two estimates of $y_{i+1}$ provides the estimate of the accuracy of the approximation.

The modified method then consists of two steps. First, the Euler method (2.54) is used to predict (compute an estimate of) $y_{i+1}$. Next this predicted value is corrected by using equation (2.56) which results in the one order better than the simple Euler method.

### 2.7.3 Runge-Kutta Methods

An important class of explicit methods called Runge-Kutta method is given by the general form:

$$\begin{aligned} k_1 &= f(x_i, y_i) \\ k_2 &= f(x_i + \beta_1 h k_1, y_i + \alpha_1 h) \\ k_3 &= f(x_i + \beta_2 h k_1 + \beta_3 h k_2, y_i + \alpha_2 h) \end{aligned}$$

$$y_{i+1} = y_i + \gamma_1 h k_1 + \gamma_2 h k_2 + \gamma_3 h k_3 + \cdots \qquad (2.57)$$

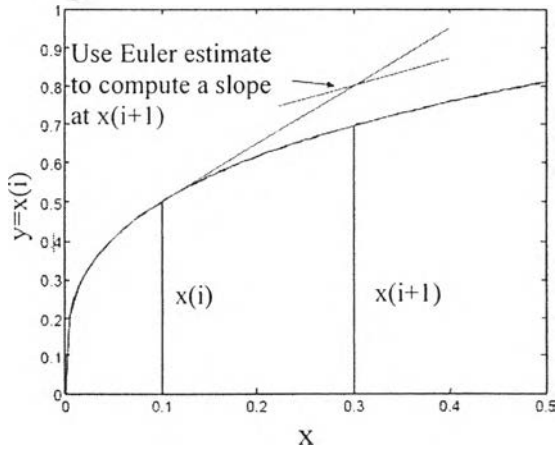


**Figure 2.49** Schematic for modified Euler method (http://www.agu.org/books/sp/057).

where the constants $\alpha_i$, $\beta_i$ and $\gamma_i$ are selected to match as many terms as possible of the exact solution :

$$y(x_{n+1}) = y(x_n) + hy'(x_n) + \frac{h^2}{2}y''(x_n) + \frac{h^3}{6}y'''(x_n) + \cdots \qquad (2.58)$$

where:

$$\begin{aligned} y' &= f \\ y'' &= f_t + ff_y \\ y''' &= f_{tt} + f_t f_y + 2ff_{yt} + f_y^2 f + f^2 f_{yy} \end{aligned}$$

Runge-Kutta method is explicit and self-starting as it does not require any information about the numerical approximation of the solution before $x_n$. This typically makes the Runge-Kutta method quite easy to use. As the number of intermediate steps $k_i$ in the Runge-Kutta method is increased, the order of accuracy of the method can also be increased.

This research presents a planned drilling operation that defines a methodology for prediction of T&D values based on soft string model and well trajectory window to reduce the potential of drilling hazards. Buckling is the main drilling problem that the developed well planning software focused on. The T&D equations were solved by Euler numerical method with a small step size because this research analyzed T&D along the straight forward of the drillstring that gives the sufficient accurate results. There are many researches involved with the analysis of T&D. Therefore, this research was developed for the knowledge of T&D analysis integrated with advanced technology development further.